Statistical properties of four-dimensional turbulence

Toshiyuki Gotoh* and Yusaku Watanabe
Department of Engineering Physics, Graduate School of Engineering, Nagoya Institute of Technology, Nagoya 466-8555, Japan

Yoshitaka Shiga and Tohru Nakano
Department of Physics, Chuo University, Tokyo 112-8551, Japan

Eijiro Suzuki
Fluent Asia Pacific Co., Ltd., Tokyo 168-8300, Japan
(Received 31 July 2006; published 22 January 2007)

The energy transfer and small-scale intermittency in decaying turbulence in four dimensions (4D) are studied by direct numerical simulation and by spectral theory in comparison with three dimensions (3D). The energy transfer is more efficient in 4D than in 3D, hence the exponent of energy decay is larger. The Kolmogorov constant is 1.31, which is smaller than 1.72 in 3D. The longitudinal third-order structure function is confirmed to be governed by a 1/2 law, $-(1/2)\bar{\varepsilon}r$, instead of a 4/5 law in 3D. The intermittency is weaker in 4D for the total dissipation rate $\nu\Sigma_{i,j}(\partial u_j/\partial x_i)^2$ and the associated velocity difference (spherical velocity difference) on scale r than in 3D, while it is slightly stronger for the surrogated dissipation rate $\nu(\partial u_1/\partial x_1)^2$ and the associated longitudinal velocity difference. The scaling exponents of the spherical and longitudinal velocity differences are also evaluated, indicating that the spherical velocity difference is less intermittent in 4D, while the longitudinal difference is more intermittent in 4D. The distribution of the eigenvalues of the strain tensor is also examined. It was also found that the normalized variance of the pressure gradient $\bar{\varepsilon}^{-3/2}\nu^{-1/2}\langle(\nabla p)^2\rangle$ in 4D is smaller than in 3D. The roles of the incompressibility condition, the pressure gradient, and the intermittency in d-dimensional turbulence are examined, and the importance of the longitudinal component of turbulent velocity field in the energy transfer toward small scales are discussed. Burgers turbulence as the asymptote of turbulence in large dimension is suggested.

DOI: 10.1103/PhysRevE.75.016310 PACS number(s): 47.27.Ak, 47.27.Jv, 47.27.Gs, 05.20.Jj

I. INTRODUCTION

Turbulence transfers energy from large to small scales of motion directly or stepwise in scale (the cascade process). As the energy is transferred downward in scale, the intermittency of the turbulent field builds up, and the scaling exponents of the velocity field deviate from Kolmogorov K41 scaling [1]. The energy transfer dynamics and intermittency are among the most important problems in the fundamental physics of turbulence. It is well known, however, that these problems have resisted solution for centuries despite many attempts to solve them.

To make progress, it is useful and important to put the problems in a wider context, for example, by relaxing the dimensional constraint, incompressibility condition, and so on. By doing so, we can find the deeper physical significance of those constraints for turbulence dynamics, which may help us to find answers to the above problems. Here we consider the effect of increasing the spatial dimension from three to four. Relevant questions are whether the energy transfer toward small scales of motion is enhanced or diminished, whether intermittency becomes stronger or weaker, and whether a critical dimension exists beyond which the scaling exponents obey K41 scaling. Some of these questions are motivated by the success of the statistical mechanical theory of critical phenomena, in which the dimension plays an essential role in understanding the physics of the fluctuations [2]. There have been a few theoretical works concerning the effects of dimension on turbulence [3–6], but no conclusive results for the effects of dimension on scaling of the energy spectrum because a simple analytical theory of turbulence which is free from arbitrary assumptions was not available and computer power was inadequate to simulate turbulence in four dimensions. During the last decade, the scaling exponents of a passive scalar field convected by an artificial Gaussian velocity field have been extensively studied. The exponents are found to approach normal scaling as the dimension increases [7–9], but our knowledge of the scaling exponents of the velocity field remains limited.

Recent dramatic increases in computer power enable us to examine the effects of the dimension on turbulence directly and to make the theoretical predictions meaningful by comparing them to numerical results [10]. This paper presents the first full report on the effects of dimension on turbulence dynamics and statistics using both direct numerical simulation (DNS) of decaying isotropic turbulence and a spectral theory of turbulence.

The findings are briefly summarized. (1) The energy transfer is more efficient in 4D than in 3D. (2) The intermittency in the energy dissipation rates depends on the type; it is weaker for the total dissipation rate in 4D, but slightly stronger for the surrogated one along a longitudinal direction. (3) The above observation indicates that we have to consider two types of the velocity differences, the usual longitudinal one and the newly introduced spherical one; the former is

*Also at CREST, Japan Science and Technology Agency, 4-1-8 Honcho, Kawaguchi, Saitama 332-0012, Japan.

more intermittent in 4D, while the latter is less so.

The present paper is organized as follows. In Sec. II the Navier-Stokes equation in any dimension is presented. The velocity derivative is expressed in the 2-form, the generalized version of the vorticity in 3D. The effects of the additional invariant are discussed, suggesting the energy cascade toward small scales. In Sec. III the energy spectrum and Kolmogorov constant in d dimensions are discussed in terms of a spectral theory of turbulence. Section IV is devoted to the DNS and the statistical properties of the simulated turbulences. In Sec. V the dimensional dependence of the Kármán-Howarth-Kolmogorov equation is studied. Degree of the intermittency of the various energy dissipation rates and velocity differences are investigated in Secs. VI and VII. To estimate the degree of the intermittency quantitatively we calculate the scaling exponents of the longitudinal and spherical velocity differences with the use of the extended self-similarity (ESS) in Sec. VIII [11]. In Sec. IX the distribution of the eigenvalues of the strain tensor is also investigated in comparison with 3D. In Sec. X the dimensional effects on the incompressibility condition and the role of the pressure gradient are discussed in relation to the intermittency and Sec. XI is the summary.

II. BASIC EQUATIONS

A. Navier-Stokes equations

The Navier-Stokes equation for an incompressible fluid with unit density in any number of space dimensions is written as

$$\frac{\partial u_i}{\partial t} + u_j \Omega_{ji} = -\frac{\partial}{\partial x_i}\left(p + \frac{u^2}{2}\right) + \nu \Delta u_i, \tag{2.1}$$

where p is the pressure and ν the kinematic viscosity, and

$$\Omega_{ij} = \frac{\partial u_j}{\partial x_i} - \frac{\partial u_i}{\partial x_j} \tag{2.2}$$

is the 2-form of the velocity field, the 4D counterpart of vorticity in 3D. Throughout this paper we employ the convention that the summation is taken over repeated indexes without stated otherwise.

Multiplying Eq. (2.1) by u_i and taking the summation over i,

$$\frac{\partial}{\partial t}\frac{1}{2}u_i^2 + \frac{\partial}{\partial x_j}\left(\frac{1}{2}u_i^2 + p\right)u_j = \nu\frac{\partial}{\partial x_j}\left(u_i\frac{\partial u_i}{\partial x_j}\right) - \nu\left(\frac{\partial u_j}{\partial x_i}\right)^2 = \nu\frac{\partial}{\partial x_j}u_i\Omega_{ji} - \frac{\nu}{2}\Omega_{ij}^2. \tag{2.3}$$

Integrating Eq. (2.3) over the entire domain and by using the homogeneous boundary condition, we find that the total energy decays in time

$$\frac{\partial}{\partial t}\int_V \frac{1}{2}u_i^2 d\boldsymbol{x} = -\frac{\nu}{2}\int_V \Omega_{ij}^2 d\boldsymbol{x} \leqslant 0. \tag{2.4}$$

Two types of the energy dissipation rates are introduced for later convenience:

$$\varepsilon(\boldsymbol{x}) = \nu\sum_{i,j}\left(\frac{\partial u_j}{\partial x_i}\right)^2, \tag{2.5}$$

$$\varepsilon'(\boldsymbol{x}) = \frac{\nu}{2}\sum_{i,j}\Omega_{ij}^2. \tag{2.6}$$

The equation for the 2-form is readily derived from Eq. (2.1) as

$$\frac{\partial}{\partial t}\Omega_{ij} + u_k\frac{\partial}{\partial x_k}\Omega_{ij} + \Omega_{ik}s_{kj} + s_{ik}\Omega_{kj} = \nu\Delta\Omega_{ij}, \tag{2.7}$$

where s_{ij} is the strain rate tensor defined as $s_{ij}=(\partial u_j/\partial x_i + \partial u_i/\partial x_j)/2$. In the framework where s_{ij} is diagonal, i.e., $s_{ij}=\lambda_i\delta_{ij}$, Eq. (2.7) becomes

$$\frac{\partial}{\partial t}\Omega_{ij} + u_k\frac{\partial}{\partial x_k}\Omega_{ij} = -(\lambda_i + \lambda_j)\Omega_{ij} + \nu\Delta\Omega_{ij}. \tag{2.8}$$

Hence the 2-form Ω_{ij} is amplified at a rate $-(\lambda_i+\lambda_j)$ in accordance with the three-dimensional case.

B. Inviscid invariants and their effects on the energy cascade

The inviscid invariants play important roles in turbulence. In two dimensions energy as well as enstrophy are conserved, and the conservation of the enstrophy prohibits the energy cascade toward high wave numbers [12,13]. According to the previous studies [14,15] there are two types of inviscid invariants depending on the parity of the dimension; in even dimensions $d=2m$, where m is an integer, the energy $E=\int(\boldsymbol{u}^2/2)d\boldsymbol{x}$ and

$$I_m[f] = \int f((dv)^m)d\boldsymbol{x} \tag{2.9}$$

are conserved, where dv is the velocity 2-form, $(dv)^m$ the antisymmetric multiple product of dv of order m, and f an arbitrary function. Since dv is nothing but the vorticity ω in two dimensions, Eq. (2.9) means that the spatial integral $f(\omega)$ is conserved. In four dimensions $(dv)^2$ is explicitly written as $(dv)^2=\Omega_{12}\Omega_{34}-\Omega_{13}\Omega_{24}+\Omega_{14}\Omega_{23}$.

In odd dimensions $d=2m+1$, on the other hand, the energy and

$$I_m = \int v \wedge (dv)^m d\boldsymbol{x} \tag{2.10}$$

are conserved. In three dimensions it is the helicity.

Assume that the velocity field with the typical velocity u_0 and wave number k_0 is initially excited. The initial transfer flux of the energy by the nonlinear interactions is $\Pi\sim k_0u_0^3$, while the initial energy dissipation rate is $\varepsilon\sim\nu|\Omega_{ij}|^2 \sim \nu(k_0u_0)^2$, by a factor $\nu k_0/u_0\sim 1/R_e$ smaller than the transfer rate. In order that the energy cascade may be realized, ε must balance Π, so that Ω_{ij} should be amplified by the factor $R_e^{1/2}$.

In two dimensions the invariant theorem states that the volume integral of any function of $dv=\Omega_{12}=\omega$ is conserved, which implies that ω^2 remains of the order of $(k_0u_0)^2$, the

initial value. Therefore the energy dissipation $\varepsilon=\nu\omega^2$ cannot match Π, meaning the prohibition of the energy transfer to small scales of motion [12,13]. It is obvious that the energy dissipation rate $\varepsilon=\nu\omega^2$ vanishes in the inviscid limit.

In the case of $d=4$, the energy dissipation is again given by the integral of the sum of the square of each component Ω_{ij} as in Eq. (2.6), assuring the positive definiteness. On the other hand, the invariant

$$I_2 = \int (dv)^2 d\boldsymbol{x} = \int (\Omega_{12}\Omega_{34} - \Omega_{13}\Omega_{24} + \Omega_{14}\Omega_{23}) d\boldsymbol{x} \tag{2.11}$$

is given by the integral of the sum of the second-order products of the form of $\epsilon_{ijkl}\Omega_{ij}\Omega_{kl}$, where ϵ_{ijkl} is the alternative unit tensor of rank 4, so that I_2 is not positive definite. It is very unlikely that the invariant I_2 (and those constructed by any function f) bounds the integral of the sum of the square of each component Ω_{ij} (i.e., the energy dissipation). With this argument and the fact that there exist terms to amplify Ω_{ij} in Eq. (2.7) [or Eq. (2.8)], it is very natural to expect that the energy dissipation ε can match the nonlinear transfer flux Π, and the energy in 4D cascades to small scales as in 3D.

In three dimensions, it is well known that there exists an invariant other than the energy, the helicity given by Eq. (2.10)

$$\int (u_1\Omega_{23} + u_2\Omega_{31} + u_3\Omega_{12}) d\boldsymbol{x} = \int \boldsymbol{u}\cdot\boldsymbol{\omega} d\boldsymbol{x} \sim O(R_e^0),$$

which is not positive definite. Since $\boldsymbol{u}$ and $\boldsymbol{\omega}$ are locally aligned at random in isotropic turbulence, the situation that ω is of order of $R_e^{1/2}k_0u_0$ but the spatial average of $\boldsymbol{u}\cdot\boldsymbol{\omega}$ is of order of $k_0u_0^2$ can be realized; the energy dissipation rate $\nu\boldsymbol{\omega}^2$ matches the energy transfer. However, it is known that the helicity attenuates the energy transfer to some extent [16,17]. From the above arguments, it seems reasonable to conclude that in 4D the energy cascades to small scales of motion as in 3D but the efficiency of the energy transfer might be different due to the inviscid invariants.

III. SPECTRAL THEORY

When turbulence is incompressible, homogeneous, and isotropic, the fundamental statistical quantity of importance is the energy spectrum. The spectral theory of turbulence provides a general view about evolution of the energy spectrum and dynamics in d dimensions. Under the periodic boundary condition with periodicity L_{box}, we expand the velocity field in terms of the Fourier series:

$$\boldsymbol{u}(\boldsymbol{x},t) = \sum_{\boldsymbol{k}} \boldsymbol{u}(\boldsymbol{k},t)e^{-i\boldsymbol{k}\cdot\boldsymbol{x}}, \tag{3.1}$$

$$\boldsymbol{u}(\boldsymbol{k},t) = \frac{1}{L_{\text{box}}^d}\int \boldsymbol{u}(\boldsymbol{x},t)e^{i\boldsymbol{k}\cdot\boldsymbol{x}} d\boldsymbol{x}. \tag{3.2}$$

When $L_{\text{box}}\to\infty$, the sum becomes the integral over the wave vectors. In the DNS study we chose $L_{\text{box}}=2\pi$, so that each component of d-dimensional wave vector $\mathbf{k}=(k_1,k_2,k_3,k_4)$ is a four-dimensional integer vector. The total energy, the energy spectral density, and the energy spectrum are defined as

$$E(t) = \frac{\langle \boldsymbol{u}^2(t)\rangle}{2} = \frac{d}{2}\bar{u}^2 = \int_0^\infty E(k,t)dk, \tag{3.3}$$

$$E(k,t) = \frac{1}{2}S_d k^{d-1}Q(k,t), \quad S_d = \frac{2\pi^{d/2}}{\Gamma(d/2)}, \tag{3.4}$$

$$\langle u_i(\boldsymbol{k},t)u_j(-\boldsymbol{k},t)\rangle = \frac{1}{d-1}P_{ij}(\boldsymbol{k})Q(k,t), \tag{3.5}$$

where $k=|\boldsymbol{k}|$, S_d is the surface area of the d-dimensional sphere of a unit radius, $\Gamma(x)$ is the Gamma function, and $P_{ij}(\boldsymbol{k})=\delta_{ij}-k_ik_j/k^2$. The energy equation is then written as

$$\left(\frac{\partial}{\partial t} + 2\nu k^2\right)E(k,t) = T(k,t), \tag{3.6}$$

where $T(k,t)$ is the energy transfer function. Energy conservation by the nonlinear term means the property

$$\int_0^\infty T(k,t)dk = 0, \tag{3.7}$$

and then the energy transfer flux is defined as

$$\Pi(k,t) = \int_k^\infty T(k',t)dk' = -\int_0^k T(k',t)dk'. \tag{3.8}$$

Also the average energy dissipation rate per unit mass is defined by

$$\bar{\varepsilon} = 2\nu\int_0^\infty k^2E(k)dk. \tag{3.9}$$

One of the difficulties of turbulence problems is that $T(k,t)$ is not expressed in a closed form. Spectral theory of turbulence yields a closed set of equations for $T(k,t)$ and has long been studied in the past. For the details, readers may refer to [18–21]. Among the spectral theories, we use the Lagrangian renormalized approximation (LRA) by Kaneda [22,23]. In LRA, (1) the energy spectral density, Lagrangian two time velocity covariance, and Lagrangian response function are fundamental quantities, (2) a closed set of equations is derived in a fully systematic way by using the renormalized expansion, therefore (3) no *ad hoc* parameters are introduced, and (4) the equations are Galilean invariant. Moreover, (5) the fluctuation-dissipation relation holds, (6) it yields the Kolmogorov scaling in the inertial range in 3D and the Kolmogorov constant 1.72 which is consistent with the experiments and DNS, and (7) it results in good predictions for low-order statistics such as the Lagrangian velocity autocorrelation, and so on [24,25]. Explanation and derivation of the LRA equations are described in Appendix A.

In this section we assume that the energy spectrum is normalized in the sense of Kolmogorov, that is, the finite energy dissipation rate $\bar{\varepsilon}$ exists and the energy spectrum is expressed in terms of the Kolmogorov variables as

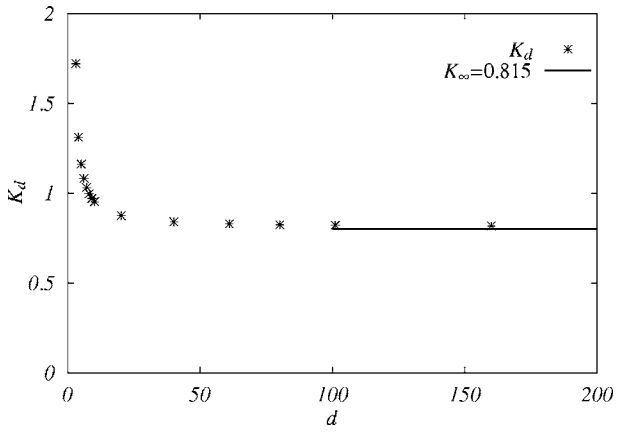

FIG. 1. Variation of the Kolmogorov constant computed by the LRA with respect to the spatial dimension d. Straight line shows the asymptotic value $K_\infty=0.815$.

$$E(k) = (\bar{\varepsilon}\nu^5)^{1/4} f(k\eta), \tag{3.10}$$

where η is the Kolmogorov length. If the Reynolds number is infinite and the intermittency effects are neglected, and if there exists the inertial range in d dimensions, then the energy spectrum is given by

$$E(k) = K_d \bar{\varepsilon}^{2/3} k^{-5/3}. \tag{3.11}$$

The LRA equations are consistent with the above scaling. We have computed the Kolmogorov constants in d dimensions in the infinite limit of the Reynolds numbers as

$$K_2 = 7.41, \quad K_3 = 1.72, \quad K_4 = 1.31, \tag{3.12}$$

where the value K_2 is the constant in the energy inverse cascading range (previously we reported as $K_4=1.28$ [10] which was slightly underestimated).

Figure 1 shows variation of the Kolmogorov constant K_d with d. The K_d is a monotonically decreasing function of d and tends to a finite value

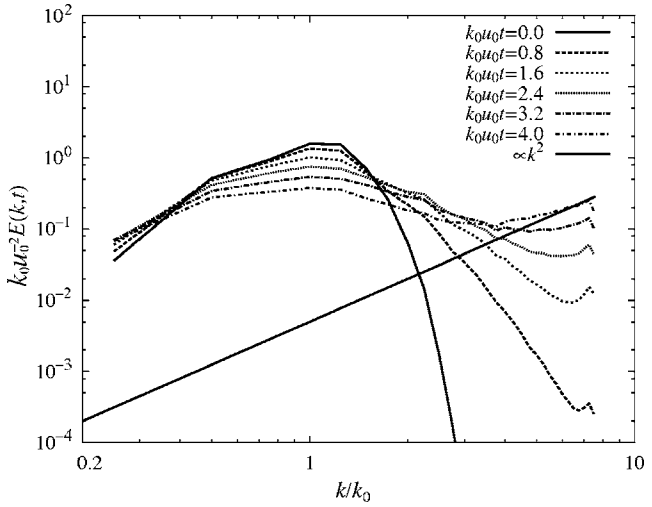

FIG. 2. Relaxation of the ITS to the equilibrium energy spectrum $E(k)\propto k^2$ in 3D.

$$K_\infty = 0.815, \tag{3.13}$$

when d becomes infinite.

The energy flux in LRA is given by

$$\Pi_d(k,t) = S_d N_d \int_k^\infty dk' \times \int\int_\Delta dpdqk'^3 (pq)^{d-2}(1-x^2)^{(d-3)/2} b_{k'pq}^{(d)} \times \int_{t_0}^t G_d(k',t,s) G_d(p,t,s) G_d(q,t,s) Q(q,s) \times [Q(p,s) - Q(k,s)] ds, \tag{3.14}$$

$$b_{kpq}^{(d)} = d\left(\frac{p}{k}\right)^2 (1-x^2) + \frac{p}{k}(2z^3 - 3z - xy), \tag{3.15}$$

$$N_d = \frac{S_{d-1}}{(d-1)^2}. \tag{3.16}$$

As described in Appendix A, when the spatial dimension d is increased, (1) $S_d N_d$ rapidly decreases for large d, (2) the geometric factor $b_{kpq}^{(d)}$ tends to be dominated by the convective term and the part arising from the pressure becomes relatively smaller, (3) the effective number of the triad interactions contributing to Π_d becomes smaller, and (4) the eddy damping factor $\mu_d(k,s')$ of the Lagrangian response function, which appears as $G_d(k,t,s)\approx\exp[-\int_s^t \mu_d(k,s')ds']$, decreases as d^{-2}.

Since $\mu_d \propto \sqrt{\langle(\nabla p)^2\rangle}$ as explained in Appendix A, the above facts (2) and (4) suggest that in the large dimensions the spectral dynamics resembles that of the passive scalar or Burgers turbulence in which the pressure term is absent and the energy is transferred only through the convective term. Therefore as far as the kinetic energy transfer is concerned, the role of the pressure becomes less and less as the spatial dimension increases.

Decrease of the eddy damping factor with the spatial dimension leads to the following effects. First, the past history of the velocity along the Lagrangian fluid particle path becomes more persistent so that the deformation of a small fluid blob also proceeds more effectively, increase of the triple relaxation time, which results in enhancement of the energy transfer to small scales. As a result, the Kolmogorov constant becomes smaller but tends to a finite constant because the above facts (1), (2), and (3) compensate the increase of the triple relaxation time. Second, the viscous effects relatively increase. Then the Kolmogorov length is given by

$$\eta_d \sim d^{3/4}\left(\frac{\nu^3}{\bar{\varepsilon}}\right)^{1/4} \tag{3.17}$$

[see Appendix A, Eq. (A31)]. The Kolmogorov length in d dimensions increases with $d^{3/4}$, implying that a much higher Reynolds number is required to attain the asymptotic inertial range.

TABLE I. DNS parameters and statistical quantities at initial time. M is the number of sampling runs. $k_{\max}\eta$ is larger than unity for all runs, the minimum value being 1.04 for Run 3C.

Run	d	Type	k_0	N	M	$10^2\nu$	E	$\bar{\varepsilon}$	R_λ	$10^2\eta$	λ/η	L/η
4A	4	I	4	64^4	2	2.00	1.97	1.59	24.7	3.99	12.5	15.6
4B	4	I	4	128^4	1	1.00	1.99	0.802	54.3	2.81	19.4	25.9
4C	4	I	4	128^4	1	0.500	2.01	0.402	110	1.99	27.6	35.8
4D	4	II	16	256^4	1	0.400	2.00	4.91	34.9	1.07	13.1	16.4
4E	4	II	16	256^4	1	0.300	2.00	3.68	46.5	0.926	15.1	18.9
4F	4	III	4	256^4	1	0.320	2.00	0.304	152	1.81	26.8	34.1
3A	3	I	4	64^3	18	2.00	1.45	1.21	24.1	5.07	9.83	12.1
3B	3	I	4	128^3	6	1.00	1.47	0.600	48.8	3.59	13.8	17.4
3C	3	I	4	128^3	6	0.500	1.48	0.300	98.6	2.54	19.5	24.5
3D	3	II	16	256^3	1	0.400	1.50	3.83	31.2	1.14	11.0	13.8
3E	3	II	16	256^3	1	0.253	1.50	2.42	49.4	0.904	13.8	17.4
3F	3	III	4	256^3	1	0.380	1.50	0.218	128	2.24	21.7	28.3
3G	3	II	32	1024^3	1	0.100	1.50	3.84	62.4	0.402	15.5	19.5

IV. DIRECT NUMERICAL SIMULATIONS AND LOW-ORDER STATISTICS

A. DNS parameters and initial conditions

The Navier-Stokes equations in three and four dimensions were numerically integrated under the periodic boundary condition with periodicity of 2π for each direction. The pseudo spectral method was used to compute the convolution sum, and the time advancing was done by the fourth-order Runge-Kutta Gill method. The details of the DNS are found in Ref. [26].

The initial random solenoidal velocity fields with given energy spectrum were generated by using the Gaussian random numbers. Three types of the initial energy spectra were used to examine the effects of the spatial dimensions on decay process, statistical invariants, spectrum evolution, and intermittency. They are

$$E_{\mathrm{I}}(k,0) = Au_0^2 k_0^{-1}(k/k_0)^4 \exp[-2(k/k_0)^2], \tag{4.1}$$

$$E_{\mathrm{II}}(k,0) = B_d u_0^2 k_0^{-1}(k/k_0)^{d+1} \exp\left(-\frac{d+1}{2}(k/k_0)^2\right), \tag{4.2}$$

$$E_{\mathrm{III}}(k,0) = B_d' u_0^2 k_0^{-1}(k/k_0)^{d+1} \exp\left[-\tfrac{1}{2}(k/k_0)^2\right]. \tag{4.3}$$

The type I spectrum with $k_0=4$ was chosen to examine the relaxation toward the absolute equipartition state of the inviscid truncated system (see the next subsection) and the decay process. For the type II spectrum, a relatively large value for the energy peak wave number $k_0=16$ was chosen in order to study the invariance of Loitsyanskii integral. The type III spectrum with $k_0=4$ was for high Reynolds number computations. We chose $u_0=1$ for all runs and the constants A, B_d, and B_d', were so chosen that the total energy was $d(u_0^2/2)$. Note that the energy per velocity component is the same in both dimensions. The spatial resolution is up to 256^3 or 256^4. The DNS parameters and the statistical quantities at initial time are given in Table I, in which L, λ, and R_λ are the integral scale, the Taylor microscale, and the Taylor microscale Reynolds number, respectively. The convergence of statistical quantities in 4D is excellent because of very large number of sample data, while that in 3D is not enough for some cases. Therefore when it was needed, the ensemble average over several (M) random initial velocity fields was taken.

TABLE II. Decay exponent of the total energy.

Run (3D)	n_{DNS}	n_{Theory}	Run (4D)	n_{DNS}	n_{Theory}
3A	1.35	1.42	4A	1.60	1.50
3D	1.33	1.42	4D	1.62	1.50
3E	1.38	1.42	4E	1.62	1.50
3G	1.42	1.42			

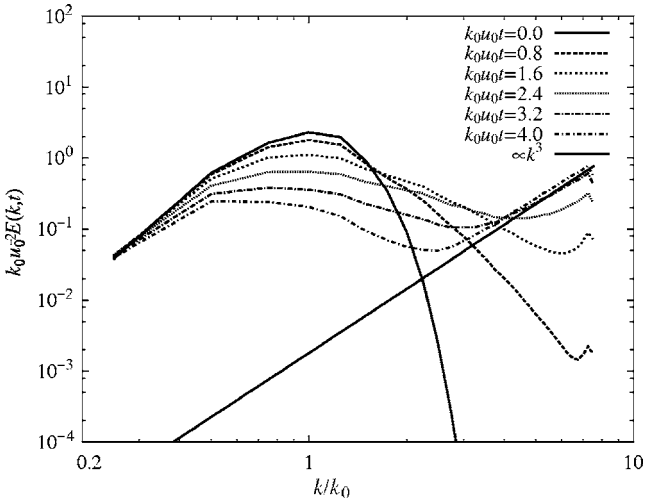

FIG. 3. Relaxation of the ITS to the equilibrium energy spectrum $E(k)\propto k^3$ in 4D.

Since the speed of the decay of turbulence differs in both dimensions, the comparison was made at times for which the Reynolds numbers were the same and as large as possible. This required extra computations to obtain appropriate parameters for fair comparison. The comparison of the spectra and statistics related to the intermittency was mostly done at the time soon after the energy dissipation attained maximum.

B. Inviscid truncated system

When the d-dimensional Euler equation is expressed in terms of the Fourier modes under the periodic boundary condition and truncated at finite wave number, such a system of the Fourier modes is the inviscid truncated system (ITS). In ITS, the invariants become very few, for example, the energy and $(dv)^2$ in 4D. If only the energy constrains the equilibrium state of ITS, then an equipartition among the Fourier modes $Q_{ij}(\boldsymbol{k})=\frac{1}{d-1}P_{ij}(\boldsymbol{k})C$ (C is a constant) is attained and leads to the absolute equilibrium energy spectrum $E_d(k) \propto k^{d-1}$ [21,27,28].

It is interesting to see whether ITS in d dimensions relaxes to the absolute equipartition state. Figures 2 and 3 show the relaxation of the energy spectrum from the initially localized spectrum (E_1) to k^{d-1} spectrum. It follows that the energy spectrum of the ITS tends to k^2 and k^3 in three and four dimensions, respectively. This means that the energy is transferred toward higher wave numbers in 4D too. The approach toward the equilibrium spectrum in 4D is seen to be faster than that in 3D, which is consistent with the efficient energy transfer in LRA prediction.

C. Energy decay and Loitsyanskii integral

The decay of the normalized turbulent energy is shown in Fig. 4. It is easily found that the decay of the total energy in 4D is faster than that in 3D, which means rapid decay of the Reynolds numbers in 4D when compared to the case in 3D (figure not shown).

When the curves of $E(t)/E(0)$ are plotted in log-log scale, there exist approximately straight portions in the curves. We fitted the curves by the formula $(t-t_0)^{-n}$, where $t_0 \approx 0$, and measured the decay exponents n's for several runs and compared in Table II. It is seen that the measured values of the decay exponents in 4D are larger than those in 3D. This is

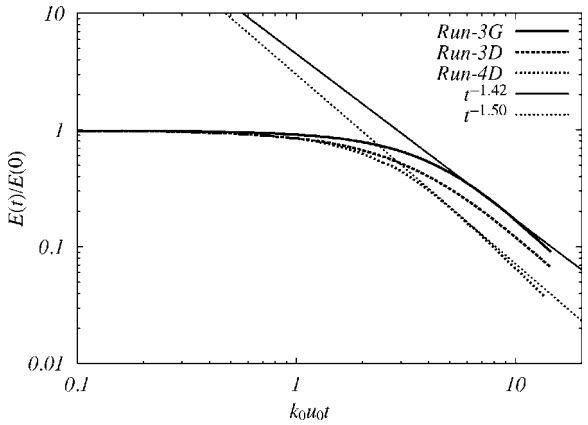

FIG. 4. The decay of the total energy. The decay exponent is larger in 4D (Run 4D) than in 3D (Runs 3D and 3G). Straight lines show the slope computed by using the Loitsyanskii integral, 1.50 for 4D and 1.42 for 3D, respectively.

consistent with the theoretical prediction which assumes invariance of the Loitsyanskii integral defined by

$$L_d(t) = 2\bar{u}^2(t)S_d\int_0^\infty r^{d+1}\hat{f}(r,t)dr, \tag{4.4}$$

where $\bar{u}^2(t)\hat{f}(r,t)=\langle \boldsymbol{u}(\boldsymbol{x}+\boldsymbol{r},t)\boldsymbol{u}(x,t)\rangle:\hat{\boldsymbol{r}}\hat{\boldsymbol{r}}$ is the longitudinal correlation function of the velocity and $\hat{\boldsymbol{r}}=\boldsymbol{r}/r$ (the mathematical details are given in Appendix B). A simple argument assuming the self-similarity of $\hat{f}$ at large-scale velocity field and the invariance of L_d yields the formula

$$n = 2(d+2)/(d+4), \tag{4.5}$$

which gives $n=10/7$ for $d=3$ and $n=3/2$ for $d=4$, respectively [29–32].

It is interesting to examine to what extent $L_d(t)$ is invariant during the decay process. It is well known that L_d is related to the coefficient of the Taylor expansion of $E(k)$ at $k=0$ as (see Appendix B)

$$E_d(k) = c_d k^{d+1} + \cdots, \tag{4.6}$$

$$c_d = \frac{S_d}{2(2\pi)^d(d+1)}m_d u_0^2 L_d, \tag{4.7}$$

TABLE III. Turbulence parameters for comparison at time $k_0u_0t=2.0$ in Runs 4A and 3A, $k_0u_0t=2.8$ in Runs 4B and 3B, and $k_0u_0t=3.4$ in Runs 4C and 3C, which are the time soon after the enstrophy has attained peak values. $[\sigma_\alpha^{(d)}]^2$, $[\sigma_\alpha^{(d)}]^2$, $S_\alpha^{(d)}$, and $K_\alpha^{(d)}$ are the variances, skewness, and flatness of the longitudinal ($\alpha=L$) and transverse ($\alpha=T$) velocity gradients, respectively.

Run	E	$\bar{\varepsilon}$	R_λ	$k_{\max}\eta$	λ/η	L/η	$[\sigma_L^{(d)}]^2$	$[\sigma_T^{(d)}]^2$	$S_L^{(d)}$	$S_T^{(d)}$	$K_L^{(d)}$	$K_T^{(d)}$
4A	1.07	1.67	13.6	1.41	8.00	13.3	3.55	5.77	−0.728	-6.35×10^{-2}	4.35	4.75
4B	1.01	1.40	20.9	1.75	10.1	20.8	5.75	9.71	−0.712	-1.35×10^{-2}	4.81	5.77
4C	1.00	1.40	29.3	1.04	12.0	30.0	11.5	19.3	−0.653	3.14×10^{-4}	4.87	6.03
3A	0.873	1.05	14.8	1.58	7.77	12.0	3.56	7.01	−0.479	-2.85×10^{-2}	3.78	4.32
3B	0.934	0.835	26.4	1.99	10.1	17.7	5.56	11.0	−0.465	-2.55×10^{-2}	4.08	5.18
3C	1.01	0.733	43.2	1.22	12.9	25.9	9.67	19.5	−0.499	1.37×10^{-2}	4.66	6.09

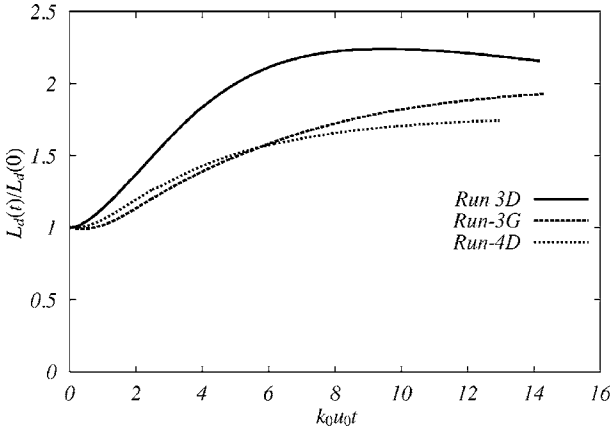

FIG. 5. Variation the Loitsyanskii integrals normalized by the initial values for Runs 3D, 4D, and 3G.

$$m_d = \int \cos^2(\theta_{kr}) d\Omega_d, \tag{4.8}$$

where θ_{kr} is the cosine of the angle between $\mathbf{k}$ and $\mathbf{r}$ and Ω_d is the solid angle in d dimensions. Then we chose the initial energy spectrum of type II which had the spectral slope $d+1$ at low wave numbers, and k_0 was chosen to be relatively large as 16, while keeping the Reynolds numbers moderate. The curve for run 3G in Fig. 5 is for reference of the accuracy of the computation, in which $k_0=32$ and larger grid points were used. The curves are approximately constant at about $k_0u_0t>4$, and correspondingly to this, the energy follows the power-law decay as seen in Figs. 4. Although it is not described in this paper, a few decay runs in 3D which started from the initial energy spectra such as $E(k,0)\propto k^m$, $m=6$ and 8 for small wave numbers were also made. It was found that the energy spectrum approached k^{d+1} for low wave numbers. Therefore we conclude that the Loitsyanskii integrals are approximately constant at late stage of evolution in both 3D and 4D within the range of Reynolds numbers studied here, and thus the decay of the total energy of turbulence obeys presumably the same law irrespective of the spatial dimensions.

TABLE IV. The scaling exponents of the longitudinal and spherical velocity differences in 3D (Run 3C) and 4D (Run 4C). The exponents are evaluated as the averages over the region $\lambda<r<L$ indicated by arrows in Figs. 19 and 20. The standard deviations are estimated as $\sigma^2=\Sigma_i(x_i-\bar{x})^2/(n-1)$ with n being the number of data points.

q	$\zeta_q^{(3)}$	$\zeta_q^{(4)}$	$\tilde{\zeta}_q^{(3)}$	$\tilde{\zeta}_q^{(4)}$
1	0.363±0.001	0.371±0.003	0.364±0.002	0.357±0.001
2	0.696±0.002	0.704±0.002	0.697±0.002	0.690±0.001
4	1.277±0.003	1.259±0.004	1.272±0.004	1.288±0.002
5	1.530±0.006	1.48±0.01	1.516±0.009	1.556±0.006
6	1.76±0.01	1.69±0.02	1.73±0.01	1.80±0.01
7	1.97±0.02	1.87±0.03	1.92±0.02	2.03±0.02
8	2.17±0.02	2.045±0.03	2.09±0.03	2.23±0.03

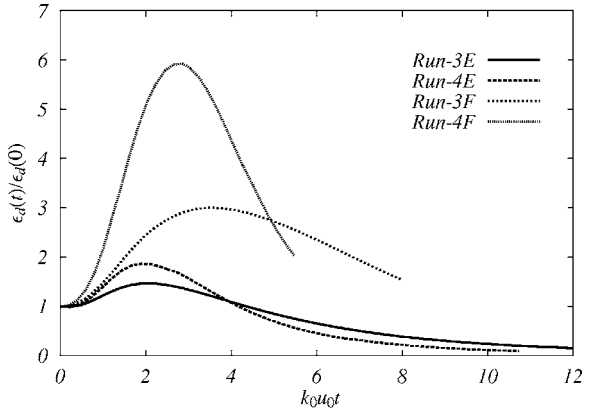

FIG. 6. Variation of the energy dissipation rate normalized by the initial value.

D. Isotropy

Most of the decaying DNS are done for the initial energy spectrum with $k_0=4$ or 16. In order to make the deviation from the isotropy at low-order moments small, when it is necessary, the average over the ensemble of the initial random velocity fields is taken. Although the precise numerical data about the isotropy of the turbulence fields in the present DNS are not available, we infer the isotropy of the low-order moments from the facts that (1) the variances of the velocity gradients $[\sigma_L^{(d)}]^2=\langle(\partial u_1/\partial x_1)^2\rangle$ and $[\sigma_T^{(d)}]^2=\langle(\partial u_1/\partial x_2)^2\rangle$ in Table III satisfy quite well the relations

$$\left\langle \left(\frac{\partial u_1}{\partial x_2}\right)^2 \right\rangle = \left(1+\frac{2}{d-1}\right)\left\langle \left(\frac{\partial u_1}{\partial x_1}\right)^2 \right\rangle, \tag{4.9}$$

which are obtained from the homogeneity, isotropy, and incompressibility conditions, (2) the small values of the skewness of the transverse velocity gradients in Table III, and (3) the small values of the third-order moments of the pressure gradients $\langle(\partial p/\partial x_1)^3\rangle$ in Table V, which should vanish under the isotropy. Therefore we consider that the isotropy of the turbulence field at small scales is at least well satisfied at low-order moments.

E. Energy dissipation rate and energy transfer

Variation of $\bar{\varepsilon}^{(d)}(t)/\bar{\varepsilon}^{(d)}(0)$ in time is shown in Fig. 6. The dissipation rates attain their maximum value at about $k_0u_0t\sim 2$ or 3. Initially, the ratio $\bar{\varepsilon}^{(4)}(0)/\bar{\varepsilon}^{(3)}(0)$ is about 4/3, but later $\bar{\varepsilon}^{(4)}(t)/\bar{\varepsilon}^{(4)}(0)$ becomes larger than $\bar{\varepsilon}^{(3)}(t)/\bar{\varepsilon}^{(3)}(0)$. When the Reynolds number becomes larger, the initial increase of $\bar{\varepsilon}^{(4)}(t)/\bar{\varepsilon}^{(4)}(0)$ becomes more significant than for 3D although $R_\lambda(0)$ in run 4F is about 20% bigger than that of run 3F. Corresponding to this, we can see in Fig. 7 that the normalized energy transfer flux function $\Pi_d(k,t)/\bar{\varepsilon}^{(d)}(t)$ is larger in 4D than in 3D for almost all wave numbers. We have observed the same tendency for other runs. These facts mean that the energy transfer in 4D is more efficient than in 3D, which is also consistent with the prediction of the spectral theory.

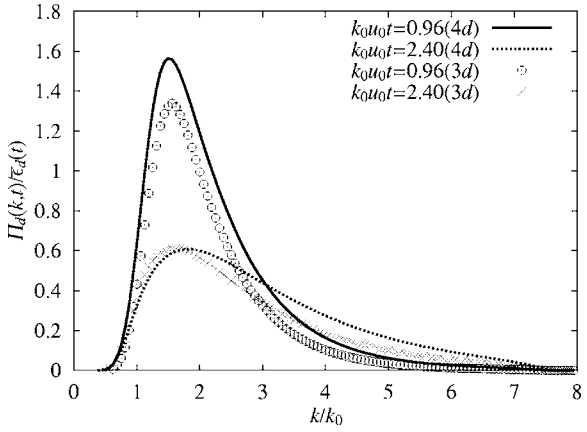

FIG. 7. Comparison of the normalized energy transfer flux at k_0u_0t=0.96 and 2.4 for runs 3E and 4E.

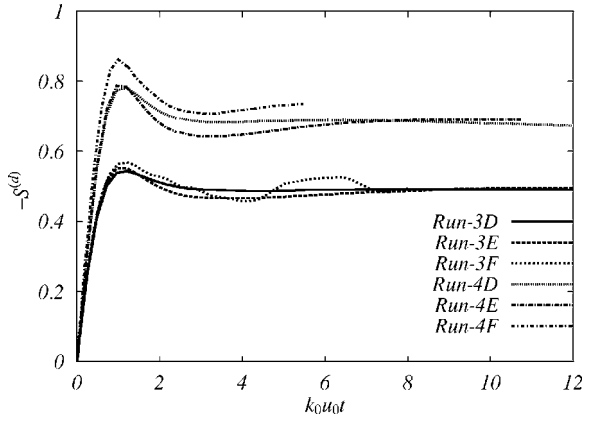

FIG. 8. Variation of the skewness $S^{(d)}$ in three and four dimensions.

Let us look at the variances of the longitudinal and transverse velocity gradients in Table III. As expected from Eq. (4.9), in 3D turbulence, the variances of the transverse velocity gradient $\partial u_1/\partial x_2$ are twice as large as those of the longitudinal ones $\partial u_1/\partial x_1$ (Runs 3A and 3C), on the other hand, in 4D turbulence, the variances of the transverse velocity gradient are $5/3 \approx 1.67$ times as large as those of the longitudinal ones (Runs 4A and 4C). Moreover, the ratio of the variance of the longitudinal to that of the transverse velocity gradient tends to unity as the spatial dimension d.

Although there is some difference in R_λ for Runs 3C and 4C, these observations suggest that the longitudinal motion of the flow field in 4D is more responsible for the energy transfer than in 3D, and bears an implication of the intermittency of the longitudinal velocity gradient stronger than that of the transverse one. In fact, we have observed that the probability density functions (PDF) normalized by the standard deviation of the longitudinal velocity gradient in 4D have slightly wider tails than in 3D, while the normalized PDF's of the transverse ones in 4D collapse well to those in 3D (figure not shown).

F. Skewness and flatness of the longitudinal velocity derivative

The skewness and flatness of the longitudinal velocity derivative are defined as

$$S^{(d)} = \frac{\left\langle \left(\frac{\partial u_1}{\partial x_1} \right)^3 \right\rangle}{\left\langle \left(\frac{\partial u_1}{\partial x_1} \right)^2 \right\rangle^{3/2}}, \quad K^{(d)} = \frac{\left\langle \left(\frac{\partial u_1}{\partial x_1} \right)^4 \right\rangle}{\left\langle \left(\frac{\partial u_1}{\partial x_1} \right)^2 \right\rangle^2}. \quad (4.10)$$

The skewness $S^{(d)}$ is a measure of the generation of small scales of motion and the energy transfer by the nonlinear term, while the flatness measures the sharpness of distribution. It follows from Fig. 8 that $S^{(4)}$ is bigger than $S^{(3)}$. Again this is consistent with the more efficient energy transfer in 4D than in 3D.

In Fig. 9, we observe that the flatness factors in both dimensions behave similarly; they start from 3, attain their maxima, and then tend to constants which are larger than 3. It should be noted that the Reynolds number dependence of $S^{(4)}$ and $K^{(4)}$ is slightly stronger than in 3D.

G. Energy spectrum

Figure 10 is a collection of the energy spectra of all runs for both dimensions in the Kolmogorov units. Collapse of the curves in both dimensions is satisfactory, which means that the Kolmogorov scaling (3.10) holds in both 3D and 4D. R_λ is too low to see the inertial range in the present DNS's. The spectrum in 4D looks the same as in 3D, but the levels of the curves of 4D at wave numbers of the inertial effect

TABLE V. Low-order statistics of the pressure gradient.

Run	k_0u_0t	R_λ	$\langle(\nabla p)^2\rangle$	$\bar{\varepsilon}^{-3/2}\nu^{1/2}\langle(\nabla p)^2\rangle$	$S_3(\nabla_x p)$	$K_4(\nabla_x p)$
3*A*	2.0	15.4	10.5	1.43	-1.31×10^{-2}	5.21
3*A*	2.4	14.6	8.20	1.36	-5.64×10^{-2}	5.43
3*A*	2.8	13.9	6.40	1.31	-9.77×10^{-2}	5.52
4*A*	2.0	14.3	12.5	0.804	-3.85×10^{-2}	5.38
4*A*	2.4	13.1	9.19	0.740	-2.64×10^{-2}	5.40
4*A*	2.8	12.2	6.62	0.692	-1.14×10^{-3}	5.36

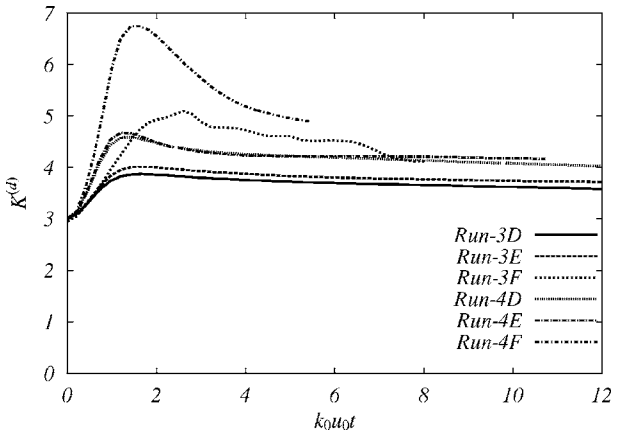

FIG. 9. Variation of the flatness $K^{(d)}$ in three and four dimensions.

dominant are lower than those of 3D. This is also consistent with the theoretical prediction in Sec. III. The inserted guiding lines represent the curves $K_d(k\eta)^{-5/3}$ with the Kolmogorov constant $K_4=1.31$ in 4D and $K_3=1.72$ in 3D, respectively. The reason for the lower value in 4D is that the energy transfer rate is larger in 4D.

V. KÁRMÁN-HOWARTH-KOLMOGOROV EQUATION

The dimensional dependence in turbulence is well elucidated in the Kármán-Howarth-Kolmogorov (KHK) equation [33–35]. The equation for arbitrary dimension d in decaying turbulence is given by

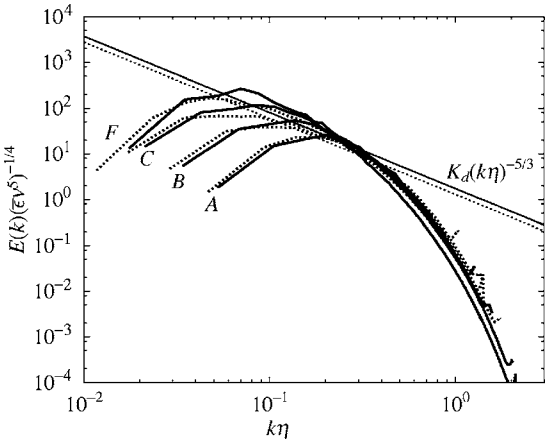

FIG. 10. A collection of the energy spectra in the Kolmogorov units for 4D and 3D. Solid lines: 3D, dashed lines: 4D. All the curves are taken soon after the enstrophy attains maximum. Runs 3A($R_\lambda=13$), 3B($R_\lambda=26$), 3C($R_\lambda=43$), 3F($R_\lambda=66$), and runs 4A($R_\lambda=14$), 4B($R_\lambda=20$), 4C($R_\lambda=29$), and 4F($R_\lambda=64$). The levels of the curves of 4D at wave numbers of the inertial effect dominant are lower than those of 3D. Straight lines stand for $K_d(k\eta)^{-5/3}$, with the Kolmogorov constants $K_3=1.72$ (solid) and $K_4=1.31$ (dotted), respectively.

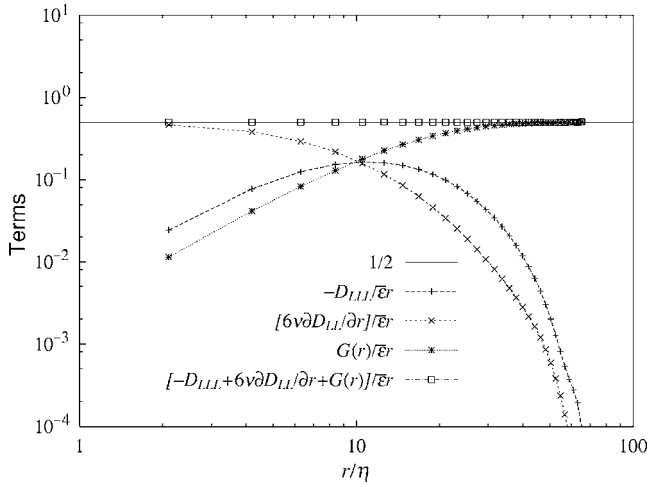

FIG. 11. A plot of each term in KHK equation for 4D (Run 4A) divided by $\bar{\varepsilon}^{(4)}r$ at $k_0u_0t=2.0$, where $G(r)=-\frac{3}{r^{d+1}}\int_0^r\frac{\partial D_{LL}(r')}{\partial t}(r')^{d+1}dr'$.

$$D_{LLL}(r)-6\nu\frac{\partial D_{LL}(r)}{\partial r}+\frac{3}{r^{d+1}}\int_0^r\frac{\partial D_{LL}(r')}{\partial t}(r')^{d+1}dr'$$

$$=-\frac{12\bar{\varepsilon}}{d(d+2)}r, \tag{5.1}$$

where $D_{LL}=\langle u_r^2\rangle$ and $D_{LLL}=\langle u_r^3\rangle$ are the second- and third-order structure functions for the longitudinal velocity increment $u_r=\hat{\boldsymbol{r}}\cdot[\boldsymbol{u}(\boldsymbol{x}+\boldsymbol{r})-\boldsymbol{u}(\boldsymbol{x})]$.

In the inertial range at infinite Reynolds number the second and third terms on the left-hand side of Eq. (5.1) can be neglected, so that $D_{LLL}=-(4/5)\bar{\varepsilon}r$ for $d=3$, while $-(1/2)\bar{\varepsilon}r$ for $d=4$. In the low Reynolds flows, however, all the terms must be retained. Figure 11 represents each term in Eq. (5.1) divided by $\bar{\varepsilon}^{(4)}r$; the KHK equation is quite satisfied as it should be. For comparison, we depicted the 3D version in Fig. 12 which is in agreement with the previous reports in DNS [26,33,36]. Note that comparisons here and in the following sections are made at the time soon after the enstrophy

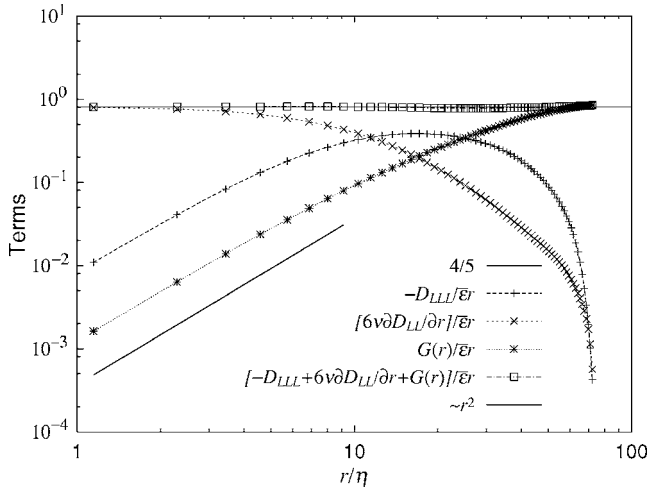

FIG. 12. A plot of each term in KHK equation for 3D (Run 3A) divided by $\bar{\varepsilon}^{(3)}r$.

has attained peak values. The turbulence parameters for comparison at these times are listed in Table III.

The skewness $S^{(d)}(r)$ for the structure function in the inertial region is evaluated in the following way. Since $D_{LLL}(r)=-12\bar{\varepsilon}r/d(d+2)$ and $D_{LL}(r)=C_d(\bar{\varepsilon}r)^{2/3}$, where C_d is connected to the Kolmogorov constant as $C_d=2.56\Gamma(d/2)K_d/\Gamma(d/2+4/3)$ [Eq. (C5) in Appendix C], the skewness becomes

$$S^{(d)}(r) = -\frac{12}{d(d+2)}\left(\frac{\Gamma(d/2+4/3)}{2.56\Gamma(d/2)}\right)^{3/2} K_d^{-3/2}. \quad (5.2)$$

The factor in front of $K_d^{-3/2}$ is a slowly increasing function of d, so that the d dependence of $S^{(d)}(r)$ is mostly affected by K_d; $S^{(d)}(r)=-0.39$ in 4D and -0.23 in 3D. When the asymptotic value of $K_\infty=0.815$ is used in Eq. (5.2), we have $S^{(\infty)}(r)\to -0.995$ in the large d limit, which is finite. The skewness of the velocity derivative is estimated from $S^{(d)}(r)$ in the limit $r\to\eta$. Reference [29] indicates that $|S^{(d)}(r)|$ increases as r decreases, resulting in the satisfactory agreement with the observation.

VI. PDF'S OF THE ENERGY DISSIPATION RATES

Since Landau's comment that the spatially inhomogeneous distribution of the energy dissipation rate may affect the scaling, PDF of the energy dissipation rate has drawn a lot of attention. In this context we investigated the PDF of the dissipation rate in 4D, in comparison with the 3D one. To cope with the fluctuations for large amplitudes, we introduced the cumulative distribution function (referred to as CDF hereafter) denoted as

$$P(>x) = \int_x^\infty P(x')dx'.$$

For the energy dissipation rates we introduce three types, because each distribution differs significantly from the others. The first one is the total energy dissipation defined by Eq. (2.5), the second the dissipation associated with the derivatives along x direction, and the third the surrogate one usually employed in the experiment:

$$\varepsilon_1(\boldsymbol{x}) = \nu\sum_{i,j}\left(\frac{\partial u_j}{\partial x_i}\right)^2, \quad (6.1)$$

$$\varepsilon_2(\boldsymbol{x}) = \nu d\sum_{j}\left(\frac{\partial u_j}{\partial x_1}\right)^2, \quad (6.2)$$

$$\varepsilon_3(\boldsymbol{x}) = \nu d(d+2)\left(\frac{\partial u_1}{\partial x_1}\right)^2. \quad (6.3)$$

The coefficients are chosen in such a way that all the averages of the above expressions are equal to $\bar{\varepsilon}$. In Fig. 13 we depicted the CDF's of ε_1, ε_2, and ε_3 in 4D, where the abscissa is normalized by $\bar{\varepsilon}$. The CDF's become broader in the sequence of ε_1, ε_2, and ε_3. It seems that the three types of the dissipation rate have been used interchangeably without paying much attention to the differences [37,38,44].

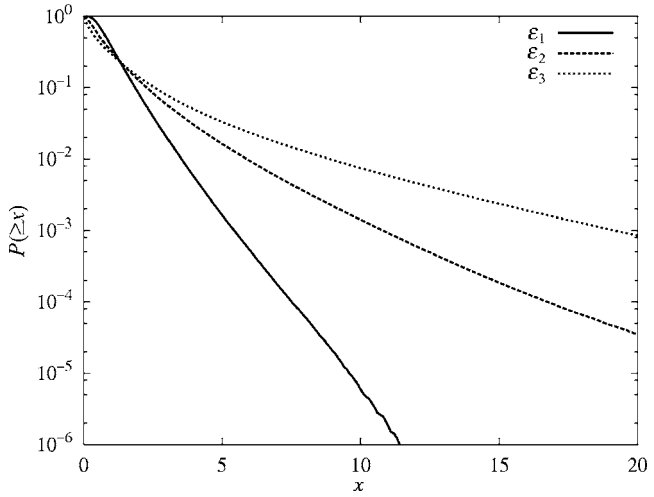

FIG. 13. CDF's of three types of the dissipation rates in 4D. The abscissa is normalized in terms of $\bar{\varepsilon}$. The CDF for ε_1 is the narrowest in the tail (Run 4A).

Figure 13 indicates that this usage is right only for the lower moments of the dissipation rate. Those CDF's for 3D show the same trend as for 4D (not depicted here).

In Fig. 14 we depicted the CDF's of ε_1 and ε_3 for 4D in parallel to those for 3D. The finding is that the CDF of ε_1 is much narrower in the tail in 4D than in 3D, while the CDF of the longitudinal components ε_3 is slightly broader in 4D than in 3D. The latter observation is consistent with the considerations discussed below on the longitudinal velocity difference, although further careful investigation is needed. The CDF's for ε_2 are almost the same for both dimensions, although they are not added to Fig. 14 for clarity.

VII. DISTRIBUTION OF THE VELOCITY INCREMENTS AND THE REFINED SELF-SIMILARITY HYPOTHESIS

When we consider the distribution of the velocity differences, they are mostly limited to the longitudinal and trans-

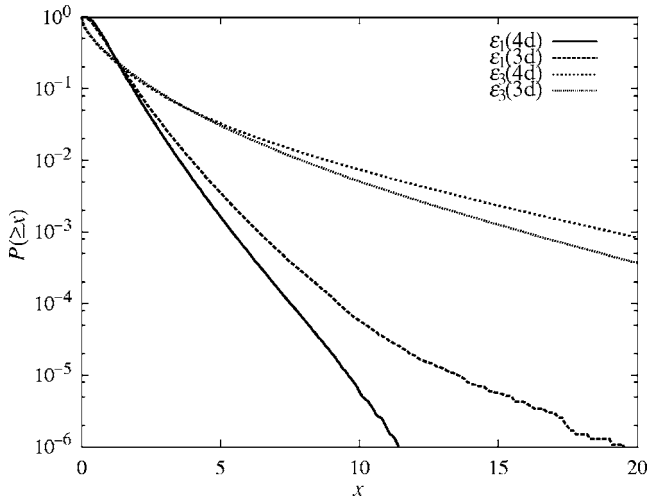

FIG. 14. CDF's of ε_1 and ε_3 for 4D (Run 4A) and for 3D (Run 3A) at $k_0u_0t=2.0$. The abscissa is normalized in terms of $\bar{\varepsilon}$.

verse ones. However, the above observation on the CDF's of the dissipation rates suggests that various types of the velocity differences are possible by extending the derivatives in Eqs. (6.1)–(6.3) to the finite differences over a distance r as

$$\frac{\partial u_j}{\partial x_i} \to \frac{u_j(\boldsymbol{x} + r\boldsymbol{e}_i) - u_j(\boldsymbol{x})}{r},$$

where $\mathbf{e_i}$ is a unit vector along i direction. Hence three types of velocity differences are defined:

$$t_1 = \sum_{i,j} [u_i(\boldsymbol{x} + r\boldsymbol{e}_j) - u_i(\boldsymbol{x})]^2, \tag{7.1}$$

$$t_2 = \sum_{i} [u_i(\boldsymbol{x} + r\boldsymbol{e}_1) - u_i(\boldsymbol{x})]^2, \tag{7.2}$$

$$t_3 = [u_1(\boldsymbol{x} + r\boldsymbol{e}_1) - u_1(\boldsymbol{x})]^2. \tag{7.3}$$

Hence t_1, t_2, and t_3 are the velocity differences corresponding to ε_1, ε_2, and ε_3 defined in Eqs. (6.1)–(6.3). t_1 represents the square of locally isotropic velocity differences over a scale r, which is referred to as the spherical velocity differences hereafter and responsible for the energy transfer in a scale space. Note that t_3 is associated with the longitudinal velocity difference and t_2 is with the sum of longitudinal and transverse differences.

Before presenting the CDF's of three types of the velocity increments we discuss the differences in those increments. Although our simulated turbulence is isotropic in the statistical sense, each domain of the strongly excited velocity fields is highly anisotropic locally. Then the velocity increment in a particular direction, say along the x direction, is the strongest, so that fluctuations of t_3 (and t_2) become larger, while t_1 would fluctuate more gently than for t_3 because t_1 is a local sum over all directions and components, the local average. The isotropic sector of the structure functions of the above three types of the velocity increments can be analyzed in terms of SO(d) decomposition as proposed by Arad *et al.* [39–41], but here we simply examined them by taking the spatial average over three (or four) directions for t_2 and t_3 because of computational cost.

Figure 15 depicts the CDF's of the velocity differences t_1 at various scales for 4D, indicating that the tail becomes narrower as the scale r increases. The CDF's of t_2 and t_3 are given in Figs. 16 and 17. Although the trend of the scale dependence in t_2 and t_3 is the same as for t_1, the decrease in the tail in t_3 is the slowest indicating that t_3, the longitudinal difference, is still very intermittent even at large r. Hence the scaling exponents of the structure functions of t_1 are expected to be very different from those of t_3. Similar trends are found for 3D, although the relevant figures are not presented here.

Figure 18 is a collection of the CDF's of t_1 and t_3 for almost the same scale; $r/\eta=8.43$ in 4D and $r/\eta=7.44$ in 3D. We found that the intermittency is weaker in the spherical velocity difference t_1 for 4D than for 3D, while the intermittency of the longitudinal velocity difference t_3 is slightly stronger for 4D than for 3D. Those tendencies are consistent with what are observed for ε_1 and ε_3.

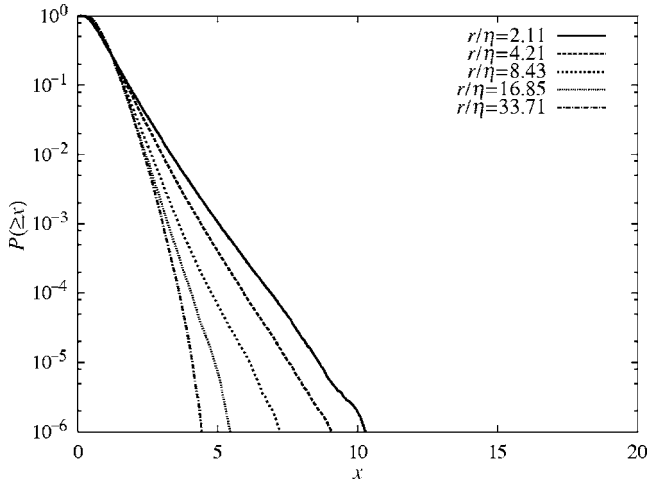

FIG. 15. CDF's of t_1 at various scales r in 4D (Run 4A). The abscissa stands for the normalized variable in terms of the mean value.

It is very important to examine the refined self-similar hypothesis under the change of the spatial dimensions. The scaling in the longitudinal velocity difference has extensively been studied. It is anticipated that the intermittency for the velocity increments is related to that for the energy dissipation rate through the refined self-similarity hypothesis [42,43]. The longitudinal velocity difference u_r over a distance r is related to the volume-averaged energy dissipation rate $\varepsilon_r(\boldsymbol{x}) = V_r^{-1} \int_{V_r} \varepsilon(\boldsymbol{x}) d\boldsymbol{x}$, where V_r is a volume over a sphere of radius r centered at $\boldsymbol{x}$, as

$$u_r \sim (r\varepsilon_r)^{1/3}.$$

Hence the less intermittent the (total) dissipation rate, the less so the longitudinal velocity increments, in contradiction with the present observation. There are two ways to reconcile the refined self-similarity hypothesis with the observations: (1) ε_3 should be used as the dissipation rate or (2) t_1 should be used as the velocity difference.

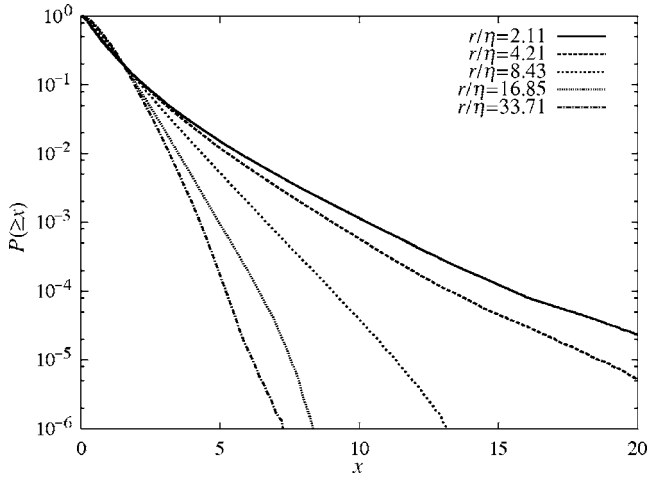

FIG. 16. CDF's of t_2 at various scales r in 4D (Run 4A). The abscissa stands for the normalized variable in terms of the mean value.

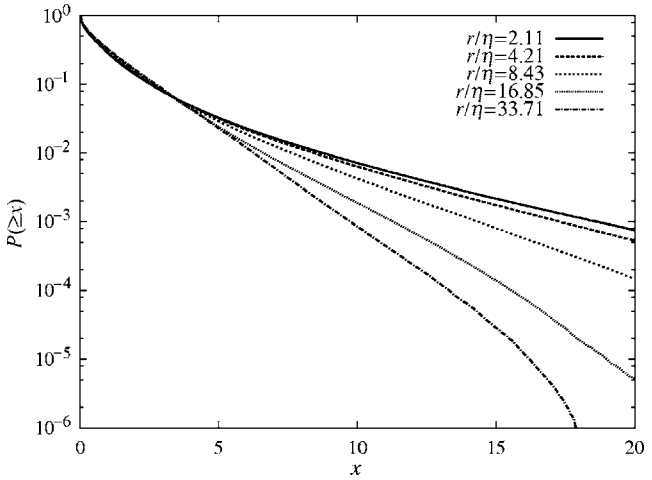

FIG. 17. CDF's of t_3 at various scales r in 4D (Run 4A). The abscissa stands for the normalized variable in terms of the mean value.

The above story also helps us to settle the long standing arguments as to which the one-dimensional dissipation surrogate or the full dissipation describes better the intermittency of the velocity increments [37,38,44]. By increasing the spatial dimensions we can find the physically relevant way to relate the velocity increments t_i to ε_i.

It is important here to note the anistopy effects. One may think that since the present DNS results are those of the decaying DNS, there might be some effects of the anisotropy arising from the relatively smaller sample sizes when compared to the case of the studies using steady turbulence. However, as we discussed before, the above analysis was done for the ensemble average over the several initial velocity fields, especially for 3D. For 4D, the statistical convergence is much better than in 3D because of the dimension 4. Therefore we infer that the effects from the anisotropy are minimized, although further examination about the anisotropy would be necessary.

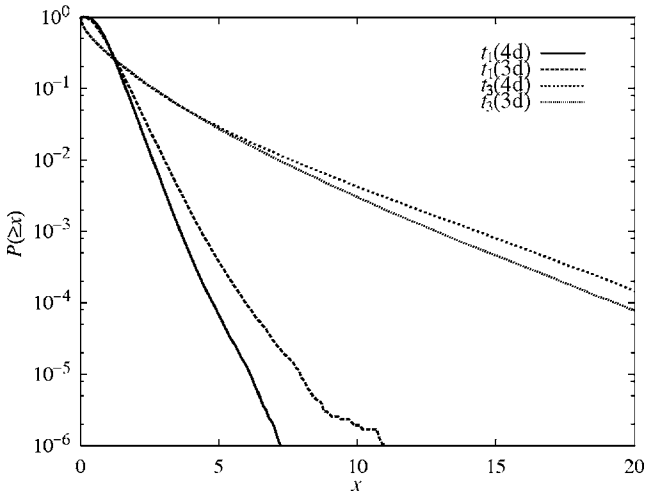

FIG. 18. CDF's of t_1 and t_3 at $r/\eta=8.43$ in 4D (Run 4A) and at $r/\eta=7.44$ in 3D (Run 3A). The abscissa stands for the normalized variable in terms of the mean value.

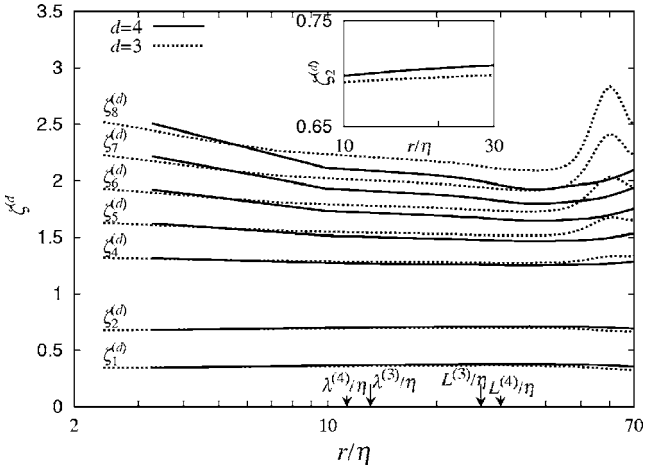

FIG. 19. Local scaling exponents $\zeta_q^{(d)}$ for the longitudinal structure functions in 4D (Run 4C) and 3D (Run 3C). The regions between two arrows are considered as the inertial effect dominant range.

VIII. SCALING OF THE VELOCITY INCREMENTS

Although the Reynolds numbers of the present DNSs are too low to observe the well-developed power-law behavior in the structure functions of the velocity increments, it is still interesting to see the general tendency of their scaling and to compare them with that in 3D.

First we argue the scaling of the longitudinal velocity increments, and then, the scaling of the spherical velocity increments. In order to obtain the reliable result of the structure functions, we process the data on one run ($R_\lambda=29.3$) on meshes 128^4 in 4D, and on six runs ($R_\lambda=43.2$) in 3D. In the following we limit ourselves to the structure functions up to order $q=8$ [45].

The longitudinal structure functions are defined for the velocity difference $u_r=\hat{\boldsymbol{r}}\cdot[\boldsymbol{u}(\boldsymbol{x}+\boldsymbol{r})-\boldsymbol{u}(\boldsymbol{x})]$ as

$$S_q^{(d)}(r)=\langle|u_r|^q\rangle, \tag{8.1}$$

where the absolute value is used instead of u_r as usual to cope with the slow convergence of the moments of odd orders. When the structure function obeys power law, we write as

$$S_q^{(d)}(r)=C_q^{(d)}(\bar{\varepsilon}r)^{q/3}\left(\frac{L}{r}\right)^{\xi_q^{(d)}}\sim r^{\zeta_q^{(d)}}. \tag{8.2}$$

Since R_λ is too low to observe the inertial range ($\lambda/\eta\sim 10$, $L/\eta\sim 30$), we must use the ESS method [11] to compute the scaling exponents $\zeta_q^{(d)}$. The local exponents calculated as

$$\zeta_q^{(d)}(r)=\frac{\mathrm{d}\log S_q^{(d)}(r)}{\mathrm{d}\log S_3^{(d)}(r)}$$

are given in Fig. 19; $\zeta_q^{(4)}<\zeta_q^{(3)}$ for $q\geqslant 4$, while $\zeta_q^{(4)}>\zeta_q^{(3)}$ for $q\leqslant 2$ as seen in the inset. This result means that the intermittency is stronger in 4D than in 3D as far as the longitudinal velocity increment is concerned.

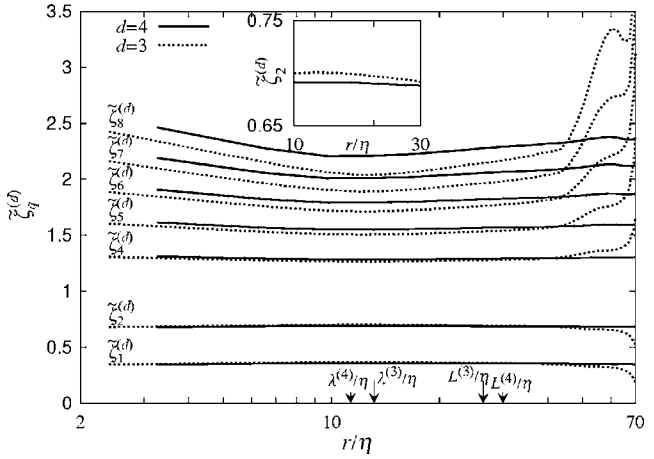

FIG. 20. Local scaling exponents $\tilde{\zeta}_q^{(d)}$ for the spherical structure functions in 4D (Run 4C) and 3D (Run 3C). The regions between two arrows are the inertial effect dominant range.

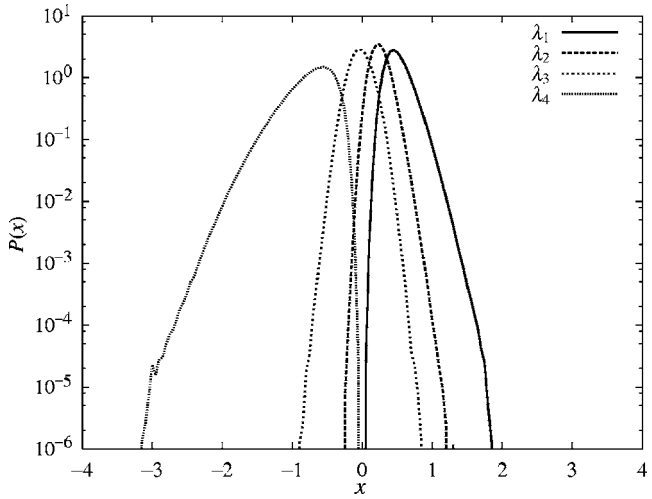

FIG. 21. PDF of eigenvalues in 4D (Run 4A). The abscissa is normalized in terms of $\sqrt{\Sigma_i\langle(\lambda_i^{(4)})^2\rangle}=\sqrt{\bar{\varepsilon}^{(4)}/\nu}$.

In the above we argued that the total dissipation rate is related to the spherical velocity differences defined in (7.1). Hence the associated structure functions are defined as

$$\tilde{S}_q^{(d)}(r)=\langle t_1(r)^{q/2}\rangle. \tag{8.3}$$

The scaling exponents $\tilde{\zeta}_q^{(d)}$ for the spherical velocity differences were calculated similarly as before by using the ESS method:

$$\tilde{\zeta}_q^{(d)}(r)=\frac{\mathrm{d}\log \tilde{S}_q^{(d)}(r)}{\mathrm{d}\log \tilde{S}_3^{(d)}(r)}.$$

Figure 20 shows that $\tilde{\zeta}_q^{(4)}>\tilde{\zeta}_q^{(3)}$ for $q\geqslant 4$, while $\tilde{\zeta}_q^{(4)}<\tilde{\zeta}_q^{(3)}$ for $q\leqslant 2$ as seen in the inset. This result means that the intermittency is weaker in 4D as far as the spherical velocity increment is concerned.

An inspection of Figs. 19 and 20 reveals that the behavior of the local scaling exponents in the spherical exponents (Fig. 20) is different from that in the longitudinal ones (Fig. 19). The former exponents are slightly increasing with r, whereas the latter ones are decreasing. This suggests that the longitudinal and spherical velocity differences may play a different role in a scale space of the energy cascade. For the longitudinal velocity difference over r the third order structure function scales proportionally to r as known in the KHK equations (5.1), supporting the ESS method in a renormalized sense. The third-order structure function of the spherical difference, on the other hand, is not directly related to the energy transfer rate, so that the ESS is not strictly justified for the spherical difference.

Even if we take into account the opposite trends of the local scaling exponents of both velocity differences, we are certain that $\tilde{\zeta}_q^{(4)}>\zeta_q^{(4)}$ for $q\geqslant 4$ and $\tilde{\zeta}_q^{(4)}<\zeta_q^{(4)}$ for $q\leqslant 2$, where the exponents are evaluated as the average values over the region $\lambda<r<L$; the numerical values are listed in Table IV, where the estimated errors are included. This indicates that the spherical velocity differences are less intermittent than the longitudinal ones, consistent with the observed trend for the various dissipation rates.

If the curves of $\zeta_q^{(3)}$ and $\tilde{\zeta}_q^{(3)}$ are plotted in the same graph, it is easily seen that they cross each other for $\lambda<r<L$. Hence we are not certain about the inequality between $\zeta_q^{(3)}$ and $\tilde{\zeta}_q^{(3)}$ at this moment. The simulation of high Reynolds number flows will elucidate the relation between those exponents. However, the following inequalities are confirmed in the present analysis:

$$\tilde{\zeta}_q^{(4)}>\tilde{\zeta}_q^{(3)},\quad \zeta_q^{(3)}>\zeta_q^{(4)},\quad \text{for } q\geqslant 4.$$

Hence the discrepancy between $\tilde{\zeta}_q^{(4)}$ and $\zeta_q^{(4)}$ is larger than that between $\tilde{\zeta}_q^{(3)}$ and $\zeta_q^{(3)}$.

IX. DISTRIBUTION OF THE EIGENVALUES OF THE STRAIN TENSOR

According to (2.8) the 2-form Ω_{ij} is amplified by $-(\lambda_i+\lambda_j)$. In three dimensions $\omega_1=\Omega_{23}$ is amplified by $-(\lambda_2^{(3)}+\lambda_3^{(3)})=\lambda_1^{(3)}$. Hence the distribution of eigenvalues is necessary to understand the microscopic structure of Ω_{ij}. First we consider the distribution in 4D, where the eigenvalues are sorted as $\lambda_1^{(4)}>\lambda_2^{(4)}>\lambda_3^{(4)}>\lambda_4^{(4)}$. The averages and the second-order moments of $\lambda_i^{(4)}$ are

$$\langle\lambda_1^{(4)}\rangle=6.60,\quad \langle\lambda_2^{(4)}\rangle=3.25,$$

$$\langle\lambda_3^{(4)}\rangle=-0.35,\quad \langle\lambda_4^{(4)}\rangle=-9.49,$$

$$\langle(\lambda_1^{(4)})^2\rangle=47.88,\quad \langle(\lambda_2^{(4)})^2\rangle=12.96,$$

$$\langle(\lambda_3^{(4)})^2\rangle=3.55,\quad \langle(\lambda_4^{(4)})^2\rangle=106.22,$$

respectively. The PDF's are shown in Fig. 21, where the abscissa is normalized in terms of $\sqrt{\Sigma_i\langle(\lambda_i^{(4)})^2\rangle}=\sqrt{\bar{\varepsilon}^{(4)}/\nu}$. For the sake of comparison we depict the PDF in 3D in Fig. 22,

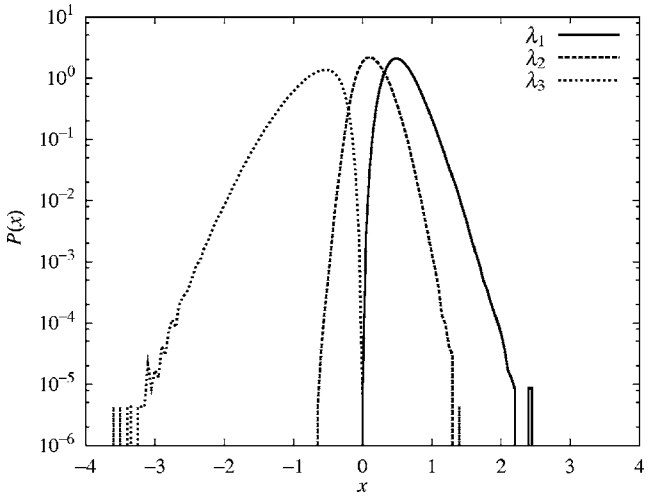

FIG. 22. PDF of eigenvalues in 3D (Run 3A). The abscissa is normalized in terms of $\sqrt{\Sigma_i \langle (\lambda_i^{(3)})^2 \rangle} = \sqrt{\bar{\varepsilon}^{(3)}/\nu}$.

where the eigenvalues are sorted as $\lambda_1^{(3)} > \lambda_2^{(3)} > \lambda_3^{(3)}$; the averages and second moments of $\lambda_i^{(3)}$ are

$$\langle \lambda_1^{(3)} \rangle = 5.74, \quad \langle \lambda_3^{(3)} \rangle = 1.51, \quad \langle \lambda_3^{(3)} \rangle = -7.24,$$

$$\langle (\lambda_1^{(3)})^2 \rangle = 37.40, \quad \langle (\lambda_2^{(3)})^2 \rangle = 5.98, \quad \langle (\lambda_3^{(3)})^2 \rangle = 63.48,$$

respectively. The abscissa is also normalized in terms of $\sqrt{\Sigma_i \langle (\lambda_i^{(3)})^2 \rangle} = \sqrt{\bar{\varepsilon}^{(3)}/\nu}$.

The following findings are obtained from the comparison of the PDF's of the eigenvalues in both dimensions. (1) The PDF of $\lambda_1^{(4)}$ is similar to that of $\lambda_1^{(3)}$. The tail is a little bit narrower in 4D as compared with 3D. (2) The PDF of $\lambda_4^{(4)}$ is very close to $\lambda_3^{(3)}$. (3) The probability of $\lambda_2^{(4)}$ being negative is considerably small. (4) The PDF of $\lambda_3^{(4)}$ is almost evenly distributed on the positive and negative sides.

An interesting comparison was found for the PDF's of fused eigenvalues. We fused the first and second eigenvalues in 4D in such a way $\lambda_1^{(4)} + \lambda_2^{(4)} \equiv \tilde{\lambda}_1^{(4)}$; the evaluated average and the second-order moments are $\langle \tilde{\lambda}_1^{(4)} \rangle = 9.84$, $\langle (\tilde{\lambda}_1^{(4)})^2 \rangle = 106.77$. Then we have three eigenvalues $\tilde{\lambda}_1^{(4)}$, $\lambda_3^{(4)}$, and $\lambda_4^{(4)}$, which are compared with $\lambda_1^{(3)}$, $\lambda_2^{(3)}$, and $\lambda_3^{(3)}$ in 3D. Figure 23 shows the comparison of $P(\tilde{\lambda}_1^{(4)})$ with $P(\lambda_1^{(3)})$, where the abscissa is normalized in terms of $\langle (\tilde{\lambda}_1^{(4)})^2 \rangle$ and $\langle (\lambda_1^{(3)})^2 \rangle$, respectively. It is surprising that the both PDF's are very close to each other. This means that $\lambda_1^{(4)}$ and $\lambda_2^{(4)}$ seem to degenerate into $\lambda_1^{(3)}$ when the dimensions decrease from four to three. Similarly we fused the second and third eigenvalues, denoted as $\lambda_2^{(4)} + \lambda_3^{(4)} \equiv \tilde{\lambda}_2^{(4)}$ [$\langle \tilde{\lambda}_2^{(4)} \rangle = 2.90$, $\langle (\tilde{\lambda}_2^{(4)})^2 \rangle = 16.05$], to compare the PDF of $\tilde{\lambda}_2^{(4)}$ with the PDF of $\lambda_2^{(3)}$ in 3D. The agreement is also good except for the left tail. Finally we constructed the PDF of the summed eigenvalue $\lambda_3^{(4)}$ and $\lambda_4^{(4)}$ denoted as $\tilde{\lambda}_3^{(4)}$ [$\langle \tilde{\lambda}_3^{(4)} \rangle = -9.84$, $\langle (\tilde{\lambda}_3^{(4)})^2 \rangle = 106.77$], which is compared with the PDF of $\lambda_3^{(3)}$ in 3D. The agreement is good except for the position of peaks.

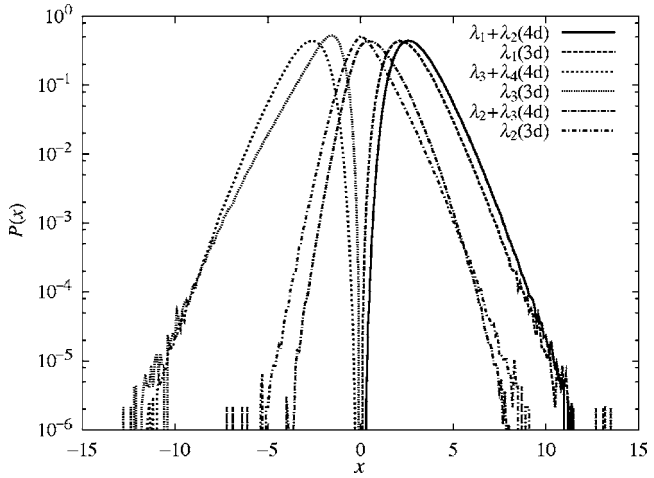

FIG. 23. The comparison of PDF's of the fused eigenvalue $\lambda_n^{(4)} + \lambda_{n+1}^{(4)}$ in 4D and $\lambda_n^{(3)}$ in 3D for $n = 1, 2, 3$. The abscissa is normalized in terms of $\sqrt{\langle (\tilde{\lambda}_i^{(4)})^2 \rangle}$ and $\sqrt{\langle (\lambda_i^{(3)})^2 \rangle}$.

X. DISCUSSION

It is interesting and important to see the effects of the spatial dimension d on the variance of the pressure gradients. For this purpose we use the quasinormal approximation and the result normalized by the Kolmogorov variables is given by

$$\bar{a}_d^2 \equiv \bar{\varepsilon}^{-3/2} \nu^{1/2} \langle (\nabla p)^2 \rangle = M_d \int_0^\infty \int_0^\infty \hat{k} \hat{p} \hat{J}_d \left(\frac{\hat{p}}{\hat{k}} \right) f(\hat{p}) f(\hat{q}) d\hat{p} d\hat{q}, \tag{10.1}$$

where Eq. (A17) is used, and the geometric factor M_d is given by Eq. (A16). Since the leading term of the function $\hat{J}_d(x)$ is x, the integral of the right-hand side of Eq. (10.1) is assumed to be weakly dependent on d. Then dimension effects are predominantly due to the geometric factor M_d. For example, $M_3/M_4 = 1.92$. Table V shows comparison of the normalized variance, skewness, and flatness of the pressure gradient for Runs 3A and 4A during their decay. The ratio $\bar{a}_3^2/\bar{a}_4^2$ is close to but about 10% smaller than 1.92. The discrepancy is due to the neglect of d dependence in $\hat{J}_d$ and the intermittency effects. The skewness' are very small and the flatness' are almost the same for both dimensions. Indeed the normalized PDF's for the pressure gradients in 3D and 4D are close to each other. It is quite interesting to observe that the normalized variance of the pressure gradient becomes smaller as d increases, although it is not certain that this trend survives at larger Reynolds numbers. This is consistent with the prediction from the spectral theory. A relatively smaller pressure gradient implies more persistent memory of fluid blob along the Lagrangian trajectory, and leads to the effective energy transfer of the energy to smaller scales. On the other hand the longitudinal velocity gradient becomes more intermittent in 4D while the transverse ones become weaker or remain unchanged.

How do we reconcile these observations? The incompressibility condition and the Navier-Stokes equation in d dimensions are written as

$$\frac{\partial u_1}{\partial x_1} + \frac{\partial u_2}{\partial x_2} + \cdots + \frac{\partial u_d}{\partial x_d} = 0, \tag{10.2}$$

$$\frac{\partial u_i}{\partial t} + u_1 \frac{\partial u_i}{\partial x_1} + u_2 \frac{\partial u_i}{\partial x_2} + \cdots + u_d \frac{\partial u_i}{\partial x_d} = -\frac{\partial p}{\partial x_i} + \nu \nabla^2 u_i. \tag{10.3}$$

When d increases, the incompressibility condition becomes less restrictive, so that there arise more chances that each longitudinal derivative can develop relatively larger amplitudes than would be for smaller d-dimensions. Now consider the convective and pressure terms in the Navier-Stokes equation. There is one longitudinal velocity gradient and $d-1$ transverse ones. When large amplitude of the longitudinal velocity gradient occurs, $d-1$ transverse terms can compensate this large squeezing or stretching action so that the sum of the convective terms, as a whole, becomes smaller and can balance with the smaller pressure gradient [46,47]. In the large limit of d, the chances are large that there exist one extreme longitudinal convective term such as $u_1 \partial u_1 / \partial x_1$ and many transverse convective terms with smaller amplitudes. The total of the convective terms would tend to obey the central limit theorem. Their sum yields the small value, and becomes comparable with the small pressure gradient. At the same time contributions from the viscous term become relatively larger. This picture resembles well the dynamics of the Burgers turbulence in which the pressure term is absent and the convective term must balance the viscous term, which leads to the formation of shocks and stronger intermittency [35,48,49].

The dissipative structure inferred from the above picture is also consistent with the CDF's for $\varepsilon_1, \varepsilon_3$. The convection dominant-dynamics of turbulence in high d dimensions steepens the longitudinal velocity gradient, then the longitudinal derivative $\partial u_1 / \partial x_1$ becomes very strong in shock regions, implying that the ε_3 is broad in the tail as seen in the CDF's of ε_3 in Fig. 14. In the region where ε_3 is strong, the other transverse components in ε_1 are rather weak but the numbers of those terms are large enough such that ε_1 tends to fluctuate gently around its mean in the sense of the central limit theorem.

The above picture explains also the observations about the velocity structure functions. When the sum is taken over the components, the energy dissipation or the pseudospherical structure function t_1 become less intermittent because of the number effects of components in the sense of the central limit theorem, for example, $d(d+1)$ for $\varepsilon^{(d)}$, while the statistics of the longitudinal component such as ε_3 and t_3 become more intermittent.

XI. SUMMARY

We have studied isotropic decaying turbulence in four dimensions. The purpose of the study is to broaden our scope on turbulence by relaxing the dimensional constraint. Emphasis was put on the energy dissipation rate, the energy transfer, and the intermittency. When the spatial dimension is increased from 3 to 4, there seems nothing dramatic. Rather, change of the nature of turbulence is gradual. However, we have found a number of important points which are useful to reconsider the physics of real turbulence in three dimensions where we live in. They are summarized as follows.

(1) Despite the existence of an infinite number of the inviscid invariants in four dimensions, the energy is transferred toward the small scales of motion due to the stretching term of velocity 2-forms.

(2) Loitsyanskii integrals are approximately constant at late stage of evolution in both 3D and 4D, and the decay of the total energy of turbulence, presumably, obeys qualitatively the same law irrespective of the spatial dimensions.

(3) However, quantitatively, there are differences in the energy transfer. The energy transfer by the nonlinear terms is more efficient in 4D than in 3D, so that the energy decays faster than in 3D and the decaying exponent in 4D is larger than in 3D, consistent with the argument in terms of the Loitsyanskii integrals.

(4) Efficient energy transfer is also predicted by the spectral theory of turbulence. The Kolmogorov constant in 4D is $K_4 = 1.31$ and tends to the finite value $K_\infty = 0.815$ for large d.

(5) Both DNS and spectral theory show that the variances of the pressure gradient decrease with increase of the spatial dimensions.

(6) In the four dimensions, Kolmogorov's 1/2 holds, which has been confirmed by the DNS when all the terms concerning the energy budgets are taken into account.

(7) The intermittency of the longitudinal velocity increments and velocity gradient becomes stronger in 4D than in 3D, while the transverse velocity gradients and the spherically averaged structure function of the velocity increments becomes less intermittent in 4D. The longitudinal motion of the velocity field becomes more responsible for the energy transfer in higher spatial dimensions.

(8) Therefore the one-dimensional surrogate of the energy dissipation exhibits stronger intermittency than it would for the full energy dissipation. This difference is attributed to the effects of the number of terms, the real dimension effects. This suggests that the refined Kolmogorov theory needs to be formulated in terms of appropriate variables, that is, the one-dimensional surrogate energy dissipation to the structure functions of the longitudinal velocity increments, or the full energy dissipation to the spherically averaged velocity structure functions.

(9) Increase of the spatial dimension leads the incompressibility condition less restrictive and more chances of extreme events for d-longitudinal velocity gradients and $d(d-1)$ terms of moderate transverse gradients. The pressure term becomes less important while the role of the viscous term increases. An implication is that the turbulence dynamics tends to follow the Burgers turbulence in large dimensions.

(10) From the above arguments, if the 4D energy spectrum $E(k)$ is computed (or measured) at high but finite Reynolds numbers, the intermittency effect on K_d would be smaller than that in 3D because of dimension effects. How-

ever, if we compute the one-dimensional energy spectrum $E_1(k_1)$ in 4D with the one-dimensional surrogate energy dissipation, the effects of the intermittency would be stronger than that in 3D.

(11) The PDF's of the eigenvalues of the rate of strain tensor in 4D are found to be similar to those would have when the middle peak of the PDF in 3d is split into two peaks.

What the above findings tell us is probably that the longitudinal velocity component plays a key role in the energy transfer than for the transverse one, which may be a good reason for the robustness (or universality) of the scaling exponents of the longitudinal structure functions, finding the same values irrespective of the differences in experimental and DNS conditions. Also we have to keep in mind in which sense we study the intermittency, the intermittency in one velocity component (one-dimensional surrogate dissipation) or the spherically averaged velocity (and the total dissipation). So far there have been many arguments in which the above difference has not been well recognized.

The DNS data and trends found in the present study were taken at relatively small or moderate Reynolds numbers, and therefore, should carefully be read. It is certainly indispensable to examine the above arguments at higher Reynolds numbers. For this purpose, the steady turbulence maintained by some energy injection mechanism is necessary. The work is in progress and will be reported.

ACKNOWLEDGMENTS

The authors express their thanks to Professor Frisch for his helpful comments and references, and Dr. Hattori for his suggestions on the inviscid invariants. Also the Theory and Computer Simulation Center, Computer and Information Network Center at National Institute for Fusion Science, and Information Technology Center of Nagoya University are acknowledged for their support to the numerical computation.

APPENDIX A: LRA EQUATIONS

The Lagrangian renormalized approximation, which is free from any adjustable parameter, enables us to calculate the Kolmogorov constant K_d for any dimension [10,22]. To understand the key points of the LRA is very useful to interpret the results of the spectral theory and to understand the dynamics and statistics of the d-dimensional turbulence. Therefore, we briefly describe the essence of the theory.

1. Fundamentals of the LRA

Lagrangian generalized velocity $\mathbf{v}(\mathbf{x},s|t)$ is defined as the velocity measured at time t of a fluid particle whose trajectory passes $\mathbf{x}$ at time s. Time argument t right of the vertical bar is called the *measuring time* while the time argument s to the left is the *labeling time* following Kraichnan's Lagrangian history direct interaction approximation (LHDIA) [50]. The dynamics of $\mathbf{v}(\mathbf{x},s|t)$ with respect to the measuring time is given by

$$\frac{\partial \boldsymbol{v}(\boldsymbol{x},s|t)}{\partial t} = \int \psi(\boldsymbol{y},t|\boldsymbol{x},s)[-\nabla p(\boldsymbol{y},t) + \nu\nabla^2 \boldsymbol{u}(\boldsymbol{y},t)]d\boldsymbol{y}, \tag{A1}$$

where $\psi(\mathbf{y},t|\mathbf{x},s)=\delta^d(\mathbf{y}-\mathbf{Z}(\mathbf{x},s|t))$ is the Lagrangian position function and $\mathbf{Z}(\mathbf{x},s|t)$ is the position of the fluid particle at time t whose trajectory passes $\mathbf{x}$ at time s. At high Reynolds numbers, the viscous term is negligible when compared to the pressure term, which means that the Lagrangian acceleration of the fluid particle is dominated by the pressure gradient. Fundamental quantities in the LRA are the energy, the Lagrangian two-time velocity covariance, and the Lagrangian response function whose equations are symbolically written as

$$\frac{\partial}{\partial t}\langle \boldsymbol{u}(\boldsymbol{x},t)\cdot\boldsymbol{u}(\boldsymbol{x}',t)\rangle = \cdots, \tag{A2}$$

$$\frac{\partial}{\partial t}\langle \boldsymbol{v}(\boldsymbol{x},s|t)\boldsymbol{v}(\boldsymbol{x}',s|s)\rangle = \cdots, \quad \text{for } t \geqslant s, \tag{A3}$$

$$\frac{\partial}{\partial t}\langle \delta\boldsymbol{v}(\boldsymbol{x},s|t)/\delta\boldsymbol{f}(\boldsymbol{x}',s|s)\rangle = \cdots, \quad \text{for } t \geqslant s, \tag{A4}$$

respectively. For details, readers may refer to [22]. In homogeneous isotropic turbulence, it is convenient to work in the wave number space. We define

$$P_{il}(\boldsymbol{k})Q_{lj}(\boldsymbol{k},s|t) = \frac{1}{d-1}P_{ij}(\boldsymbol{k})Q(k,t,s), \tag{A5}$$

$$P_{il}(\boldsymbol{k})G_{lm}(\boldsymbol{k},s|t)P_{mj}(-\boldsymbol{k}) = P_{ij}(\boldsymbol{k})G(k,t,s), \tag{A6}$$

$$Q(k,t) = Q(k,t,t). \tag{A7}$$

The renormalized expansions yield a closed set of equations. Then the LRA equations in the wave number space are the energy equation

$$\left(\frac{\partial}{\partial t} + 2\nu k^2\right)Q(k,t) = 2N_d k^{4-d} \times \int\int_{\Delta} dpdq(pq)^{d-2}(1-x^2)^{(d-3)/2}b_{kpq}^{(d)} \times \int_{t_0}^{t} G_d(k,t,s)G_d(p,t,s)G_d(q,t,s)Q(q,s) \times [Q(p,s)-Q(k,s)]ds, \tag{A8}$$

$$b_{kpq}^{(d)} = \frac{p}{k}[d(z+xy)+2z^3-3z-xy], \tag{A9}$$

$$N_d = \frac{S_{d-1}}{(d-1)^2}, \tag{A10}$$

the fluctuation-dissipation relation for the two-time velocity covariance

$$Q(k,t,s) = G_d(k,t,s)Q(k,s,s), \tag{A11}$$

and the Lagrangian response equation

$$\left(\frac{\partial}{\partial t} + \nu k^2 + \mu_d(k,t,s)\right)G_d(k,t,s) = 0, \quad t \geqslant s \tag{A12}$$

$$\mu_d(k,t,s) = \int_0^\infty dpkpJ_d\left(\frac{p}{k}\right)\int_s^t G_d(p,t,s')E(p,s')ds', \tag{A13}$$

$$J_d(x) = M_d\hat{J}_d(x), \tag{A14}$$

$$\hat{J}_d(x) = \hat{J}_d(1/x) = \begin{cases} xF(1,-d/2,d/2+2,x^2), & x \leqslant 1 \\ \dfrac{1}{x}F(1,-d/2,d/2+2,1/x^2), & x > 1 \end{cases} \tag{A15}$$

$$M_d = \frac{4S_{d-1}}{(d-1)^2 S_d}B\left(\frac{d+3}{2},\frac{1}{2}\right), \tag{A16}$$

where F is Gauss' hypergeometric function, B is the beta function, and (x,y,z) are the cosines of the interior angles opposite the triangle sides (k,p,q), respectively. As in 3D, the detailed balance, and the energy conservation by the nonlinear term hold.

It is very important to anticipate the fact that corresponding to Eq. (A1), the eddy damping factor μ_d in Eq. (A12) arises from the Lagrangian mapping of the pressure gradient. In fact, if the quasinormal approximation is applied to the variance of the pressure gradient, we obtain

$$\langle(\nabla p)^2\rangle = \int_0^\infty\int_0^\infty kpJ_d\left(\frac{p}{k}\right)E(p)E(q)dpdq, \tag{A17}$$

which is identical to Eq. (8.3.20) of Batchelor [51].

The eddy damping factor μ_d is a key to the spectral dynamics. If we assume that the turbulence is in a steady state, then $G_d(k,t,s)$ is a function of $t-s$. Furthermore we truncate F in Eq. (A14) at the zeroth order, i.e., $F=1$, and integrate in time from infinite past to the present time t, we arrive at

$$\mu_d(k) \approx \sqrt{M_d}\left(\int_0^k p^2E(p)dp + k^2\int_k^\infty E(p)dp\right)^{1/2}. \tag{A18}$$

This means that in d dimensions the eddy damping at scale $1/k$ is roughly given by the total strain from scales of motion larger than $1/k$ and by the excitation of scales smaller than $1/k$, which is consistent with the case in 3D.

If there exists the inertial range in the sense of Kolmogorov (1941) at very high Reynolds number, we have the following similarity form:

$$E(k) = K_d\bar{\varepsilon}^{2/3}k^{-5/3}, \quad G_d(k,\tau) = \bar{G}_d(\bar{\varepsilon}^{1/3}k^{2/3}\tau), \tag{A19}$$

where K_d is the Kolmogorov constant in d dimensions, and $\tau=t-s$. In the inertial range the energy transfer flux is expressed as

$$\bar{\varepsilon} = \Pi_d(k) = \bar{\varepsilon}K_d^{3/2}\frac{4dS_{d-1}}{(d-1)^2S_d\sqrt{M_d}}\bar{A}_d, \tag{A20}$$

$$\bar{A}_d = \int_0^1 du\,\log(1/u)\int_{\max(u,|1-u|)}^{u+1} dv\bar{\Theta}_d(1,u,v)\bar{D}_d(1,u,v), \tag{A21}$$

where

$$\bar{D}_d(1,u,v) = (1-x^2)^{(d-3)/2}u^{-8/3}[(\bar{b}_{1uv}^{(d)} + \bar{b}_{1vu}^{(d)})v^{-8/3} - (\bar{b}_{1uv}^{(d)}u^{d+2/3}v^{-8/3} + \bar{b}_{1vu}^{(d)}v^{d-2})], \tag{A22}$$

$$b_{1uv}^{(d)} = d\bar{b}_{1uv}^{(d)} = d\left(u^2(1-x^2) + \frac{u}{d}(2z^3-3z-xy)\right), \tag{A23}$$

$\bar{\Theta}_d$ is the triple relaxation time defined by

$$\bar{\Theta}_d(1,u,v) = \int_0^\infty \bar{G}_d(s)\bar{G}_d(u^{2/3}s)\bar{G}_d(v^{2/3}s)ds, \tag{A24}$$

in which $\bar{G}_d(\sigma)=G_d(\sqrt{M_d}\bar{\varepsilon}^{1/3}k^{2/3}\tau)$ obeys

$$\frac{d\bar{G}_d(\sigma)}{d\sigma} + \left(\int_0^\infty dxx^{-2/3}\hat{J}_d(x)\int_0^\sigma d\xi\bar{G}_d(x^{2/3}\xi)\right)\bar{G}_d(\sigma) = 0. \tag{A25}$$

$\bar{A}_d$ can be evaluated numerically so that K_d is computed as function of d as found in Fig. 1. The Kolmogorov constant K_d remains finite in the large limit of d.

2. Asymptotic behavior for large dimensions

When d is very large, the geometric factor $b_{1uv}^{(d)}$ and the eddy damping factor μ_d become

$$b_{1uv}^{(d)} \sim du^2(1-x^2), \tag{A26}$$

$$\mu_d(k,\tau) \sim \frac{4}{d^2}\int_0^\tau ds'\int_0^\infty dpkp\hat{J}_\infty\left(\frac{p}{k}\right)E(p)G_d(p,s') \equiv \frac{4}{d^2}\hat{\mu}_\infty(k,\tau), \tag{A27}$$

$$\hat{J}_\infty(x) = \hat{J}_\infty(1/x) = \frac{x}{1+x^2}. \tag{A28}$$

It is very interesting and important to see that

(1) in the large limit of d the geometric factor tends to $\bar{b}_{1uv}^{(d)}=u^2(1-x^2)$ which is given by the convective term alone,

(2) the eddy damping term arising from the pressure gradients becomes small as d^{-2}.

These two points suggest that in the large dimensions the spectral dynamics comes to resemble that of the Burgers or passive scalar turbulences.

Equation (A12) of the response function for large d becomes

$$\left(\frac{\partial}{\partial\xi}+d\nu k^2+\hat{\mu}_\infty(k,\xi)\right)G_d(k,\xi)=0,\quad \xi=\pi/d. \tag{A29}$$

In the inertial range, the viscous damping term is negligible when compared to the eddy damping term, which requires

$$\nu=o(1/d). \tag{A30}$$

Alternatively this can be stated as follows. If the Kolmogorov scale is defined as the time at which the viscous dissipation time becomes comparable with the eddy damping term, then we have an estimate

$$\eta_d\sim d^{3/4}\left(\frac{\nu^3}{\bar{\varepsilon}}\right)^{1/4}. \tag{A31}$$

The Kolmogorov length in d dimensions increases with $d^{3/4}$, implying that much higher Reynolds number is required to attain the asymptotic inertial range, or the molecular dissipation effects become stronger with increase of the dimensions.

When the asymptotic form of the response function in the large d limit is inserted into Eq. (A24), we obtain

$$\hat{\Theta}_{1uv}=\lim_{d\to\infty}\bar{\Theta}_d(1,u,v)=\int_0^\infty g(s)g(u^{2/3}s)g(v^{2/3}s)ds, \tag{A32}$$

$$g(s)=\lim_{d\to\infty}\bar{G}_d(s), \tag{A33}$$

and then substituting this into Eq. (A21) we arrive at

$$K_d=\left[\frac{(d-1)^2S_d}{4d^2S_{d-1}}B\left(\frac{d+3}{2},\frac{1}{2}\right)\right]^{1/3}\bar{A}_d^{-2/3}\sim\left(\frac{\pi}{2}\right)^{1/3}(d^{1/2}\bar{A}_d)^{-2/3}. \tag{A34}$$

In order to compute the integral $\bar{A}_d$, we use the steepest decent method for the integral over v. It follows that when d becomes very large the geometric factor $(1-x^2)^{(d-3)/2}=[\sin(\theta_k)]^{(d-3)/2}$ has nonzero contributions only from the set satisfying $\theta_k\approx\pi/2$, where θ_k is the angle opposite to the side k of the triangle (k,p,q). This means that there are two paths; Γ_1 is the path $\{(u,v):u^2+v^2=1\}$ for the first term in the square brackets of Eq. (A22), and Γ_2, $\{(u,v):v^2=1+u^2\}$ for the second term [6]. The results are

$$\bar{A}_d\sim\left(\frac{2\pi}{d}\right)^{1/2}I, \tag{A35}$$

$$I=\int_0^1\log\left(\frac{1}{u}\right)u^{-5/3}[(1-u^2)^{-4/3}\hat{\Theta}_{1u\sqrt{1-u^2}}H(\sqrt{2}/2-u)-\hat{\Theta}_{1u\sqrt{1+u^2}}]du\approx 0.680, \tag{A36}$$

where $H(x)$ is the Heaviside function. The numerical computation of Eq. (A36) yields the asymptotic value of the Kolmogorov constant in the infinite dimensions as $K_\infty=0.815$ which is shown in Fig. 1.

As seen in the asymptotic analysis described above, the increase of the spatial dimension implies that the number of the triad interaction contributing to the energy transfer becomes fewer while the decay of the response function gets slower so that the triple relaxation time becomes larger. As a result both effects are compensated and lead to the finiteness of the Kolmogorov constant in the large d limit.

APPENDIX B: LOITSYANSKII INTEGRALS AND DECAY EXPONENT

The decay exponent might be interpreted in the following way [29,30,32]. Let us put the typical velocity and scale as

$$u(t)\sim(t-t_0)^m,\quad \ell(t)\sim(t-t_0)^{m+1}. \tag{B1}$$

The decaying exponent, then, becomes $n=-2m$. We have to evaluate m. Suppose that the decaying turbulence is self-similar, i.e., $B_{LL}(r,t)=\langle\boldsymbol{u}(\boldsymbol{x}+\boldsymbol{r},t)\boldsymbol{u}(\boldsymbol{x},t)\rangle:\hat{\boldsymbol{r}}\hat{\boldsymbol{r}}=\bar{u}^2(t)\hat{f}(r/\ell(t))$, where $\hat{f}$ is a certain function. If $B_{LL}(r)$ and $B_{LL,L}(r)=\langle\boldsymbol{u}(\boldsymbol{x}+\boldsymbol{r},t)\boldsymbol{u}(\boldsymbol{x},t)\boldsymbol{u}(\boldsymbol{x},t)\rangle\hat{\boldsymbol{r}}\hat{\boldsymbol{r}}\hat{\boldsymbol{r}}$ decay faster than r^{-d-2} and r^{-d-1} for $r\to\infty$, the Loitsyanskii invariant L_d defined by

$$L_d(t)=2\bar{u}^2(t)S_d\int_0^\infty r^{d+1}\hat{f}(r)dr \tag{B2}$$

is independent of t even in decaying turbulence [29,30,32]. Substituting Eq. (B1) into Eq. (B2) yields

$$L_d\sim(t-t_0)^{2m+(m+1)(d+2)},$$

from which $m=-(d+2)/(d+4)$. Hence the decaying exponent becomes

$$n=2(d+2)/(d+4), \tag{B3}$$

giving $n=10/7$ for $d=3$, while $n=3/2$ for $d=4$, which accord roughly with the fitted values $n=1.35$ for $d=3$ and 1.60 for $d=4$.

In order to express the Loitsyanskii integral in a spectral theory we introduce the relation between the longitudinal velocity correlation $B_{LL}(r)$ in coordinate space and the transverse correlation function $F_{NN}(k)=\langle|\boldsymbol{u}(\boldsymbol{k})|^2\rangle(2\pi)^d/L_{\mathrm{box}}^d$ in wave number space. For arbitrary dimensions d we have

$$F_{NN}(k)=\frac{2S_{d-1}}{(2\pi)^d}\int drr^{d-1}B_{LL}(r)\int_0^1 d\mu(1-\mu^2)^{(d-3)/2}\times\left(\mu\frac{\sin kr\mu}{kr}-\frac{1}{d-1}[(1-\mu^2)\cos(kr\mu)-kr\mu\sin(kr\mu)]\right).$$

To this end the left-hand side is expanded in terms of power of k^2 as

$$F_{NN}(k)=f_0+f_1k^2+\cdots.$$

Expanding the right-hand side in powers of k^2 yields that $f_0=0$, while f_1 is nonzero:

$$f_1 = \frac{6}{d-1}\frac{\pi^{d/2}}{\Gamma\left(\frac{d}{2}+2\right)}\int dr r^{d+1} B_{LL}(r). \tag{B4}$$

Thus the existence of the Loityanskii invariant is equivalent to the existence of f_1, i.e., $F_{NN}(k) \sim k^2$. Then, the energy spectrum must be $E(k,t) \propto k^{d+1}$.

APPENDIX C: THE RELATION BETWEEN THE COEFFICIENTS OF $D_{LL}(r)$ AND $E(k)$

Here we present some useful relations in d-dimensional turbulence. First we define

$$D_{LL}(r) = C_d(\bar{\varepsilon} r)^n, \quad E(k) = K_d \bar{\varepsilon}^n k^{-n-1}. \tag{C1}$$

Then

$$D_{LL}(r) = \sum_{\boldsymbol{k}} |\boldsymbol{e}^{ik_1 r} - 1|^2 \langle |u_1(\boldsymbol{k})|^2 \rangle$$

$$= \frac{4}{(d-1)S_d}\int d\boldsymbol{k}_\perp dk_1 \left(1 - \frac{k_1^2}{k^2}\right)(1 - \cos k_1 r)\frac{E(k)}{k^{d-1}}.$$

Substituting $d\boldsymbol{k}_\perp = S_{d-1} k_\perp^{d-2} dk_\perp$, we have

$$D_{LL}(r) = \frac{8S_{d-1}}{(d-1)S_d}\int_0^\infty (1 - \cos k_1 r) A_d(k_1) dk_1,$$

where

$$A_d(k_1) = \int_0^\infty dk_\perp \frac{k_\perp^d}{(k_\perp^2 + k_1^2)^{(d+1)/2}} E(\sqrt{k_\perp^2 + k_1^2}).$$

Substituting $q^2 = k_1^2 + k_\perp^2$, $qdq = k_\perp dk_\perp$ yields

$$A_d(k_1) = \int_{k_1}^\infty dq q \frac{(q^2 - k_1^2)^{(d-1)/2}}{q^{d+1}} E(q)$$

$$= \frac{1}{2} K_d \bar{\varepsilon}^n k_1^{-n-1} B\left(\frac{n+1}{2}, \frac{d+1}{2}\right).$$

Then

$$D_{LL} = \frac{4S_{d-1}K_d}{(d-1)S_d}\bar{\varepsilon}^n B\left(\frac{n+1}{2}, \frac{d+1}{2}\right) F_n, \tag{C2}$$

where

$$F_n = \int_0^\infty k_1^{-n-1}(1 - \cos k_1 r) dk_1. \tag{C3}$$

Then after the partial integration we have

$$F_n = \frac{r^n}{n(1-n)}\Gamma(2-n)\sin\left(\frac{\pi}{2}(1-n)\right). \tag{C4}$$

Substituting $n = 2/3$, we have $F = 2.01 r^{2/3}$:

$$\frac{C_d}{K_d} = \frac{8.04 S_{d-1}}{(d-1)S_d} B\left(\frac{n+1}{2}, \frac{d+1}{2}\right).$$

We go further. Since $S_d = 2\pi^{d/2}/\Gamma(d/2)$, we have

$$\frac{C_d}{K_d} = 2.56\frac{\Gamma(d/2)}{\Gamma(d/2 + 4/3)}, \tag{C5}$$

where the formula $B(x,y) = \Gamma(x)\Gamma(y)/\Gamma(x+y)$ has been used.

Let us focus on a large value of d. The asymptotic form of $\Gamma(z)$ is

$$\log \Gamma(z) \sim \frac{1}{2}(\log 2\pi - 1) - z - \log z$$

$$+ \left(\frac{z}{2} + \frac{1}{4}\right)[\log z + \log(z+1)] + \frac{1}{12}\log\frac{z+1}{z}.$$

Then we have

$$\log \Gamma(z) - \log \Gamma(z + 4/3) \sim -\frac{4}{3}\log z.$$

Finally we are led to

$$\frac{C_d}{K_d} = 6.54 d^{-4/3}. \tag{C6}$$

[1] A. N. Kolmogorov, Dokl. Akad. Nauk SSSR **30**, 9 (1941).
[2] K. G. Wilson, Phys. Rev. B **4**, 3174 (1971).
[3] M. Nelkin, Phys. Rev. A **9**, 388 (1974); **11**, 1737 (1975).
[4] P. G. de Gennes, in *Proceedings of the NATO Advanced Study Institute on Fluctuations, Instabilities, and Phase Transitions*, edited by T. Riste (Plenum Press, New York, 1975), p. 1.
[5] J. D. Fournier and U. Frisch, Phys. Rev. A **17**, 747 (1978).
[6] J. D. Fournier, U. Frisch, and H. A. Rose, J. Phys. A **11**, 187 (1987).
[7] R. H. Kraichnan, Phys. Rev. Lett. **72**, 1016 (1994).
[8] M. Chertkov, G. Falkovich, I. Kolokolov, and V. Lebedev, Phys. Rev. E **52**, 4924 (1995).
[9] G. Falkovich, K. Gawedzki, and M. Vergassola, Rev. Mod. Phys. **73**, 913 (2001).
[10] E. Suzuki, T. Nakano, N. Takahashi, and T. Gotoh, Phys. Fluids **17**, 081702 (2005).
[11] R. Benzi, S. Ciliberto, R. Tripiccione, C. Baudet, F. Massaioli, and S. Succi, Phys. Rev. E **48**, R29 (1993).
[12] G. K. Batchelor, Phys. Fluids **12**, 233 (1969).
[13] R. H. Kraichnan, Phys. Fluids **10**, 1417 (1967).
[14] B. A. Khesin and Yu. V. Chekanov, Physica D **40**, 119 (1989), preceding references are therein.
[15] S. Gama and U. Frisch, in *1993 Proceedings of NATO-ASI: Solar and Planetary Dynamos*, Cambridge, edited by M. R. E. Proctor, P. C. Mathews, and A. M. Rucklidge (Cambridge University Press, Cambridge, 1993), pp. 115–119.
[16] R. H. Kraichnan, J. Fluid Mech. **59**, 745 (1973).
[17] J. C. Andre and M. Lesieur, J. Fluid Mech. **81**, 187 (1977).
[18] D. C. Leslie, *Developments in the Theory of Turbulence* (Clarendon, Oxford, 1973).

[19] M. Lesieur, *Turbulence in Fluids*, 2nd ed. (Kluwer, Dordrecht, 1990).
[20] W. D. McComb, *The Physics of Fluid Turbulence* (Oxford University Press, Oxford, 1990).
[21] T. Gotoh, *Fundamentals in the Theory of Turbulence* (in Japanese) (Asakura, Tokyo, 1998).
[22] Y. Kaneda, J. Fluid Mech. **107**, 131 (1981).
[23] Y. Kaneda, Phys. Fluids **29**, 701 (1986).
[24] Y. Kaneda and T. Gotoh, Phys. Fluids A **3**, 1924 (1991).
[25] T. Gotoh and Y. Kaneda, Phys. Fluids A **3**, 2426 (1991).
[26] T. Gotoh, D. Fukayama, and T. Nakano, Phys. Fluids **14**, 1065 (2002).
[27] S. A. Orszag, *Lectures in the Statistical Theory of Turbulence*, Les Houches Summer School of Theoretical Physics, edited by R. Balian and J. L. Peube (Gordon and Breach, New York, 1977).
[28] Y. Kaneda and T. Gotoh, Phys. Fluids A **1**, 1225 (1989).
[29] A. S. Monin and A. M. Yaglom, *Statistical Fluid Mechanics* (MIT Press, Cambridge, MA, 1975), Vol. 2, p. 177.
[30] U. Frisch, *Turbulence* (Cambridge University Press, Cambridge, 1995).
[31] M. Oberlack, Proc. Appl. Math. Mech. **1**, 294 (2002).
[32] P. A. Davidson, *Turbulence* (Oxford University Press, Oxford, 2004).
[33] D. Fukayama, T. Oyamada, T. Nakano, T. Gotoh, and K. Yamamoto, J. Phys. Soc. Jpn. **69**, 701 (2000).
[34] R. J. Hill, J. Fluid Mech. **434**, 379 (2001).
[35] V. Yakhot, Phys. Rev. E **63**, 026307 (2001).
[36] L. Danaila, F. Anselmet, T. Zhouand, and R. A. Antonia, J. Fluid Mech. **391**, 359 (1999).
[37] G. Stolovitzky, P. Kailasnath, and K. R. Sreenivasan, Phys. Rev. Lett. **69**, 1178 (1992).
[38] G. Stolovitzky and K. R. Sreenivasan, Rev. Mod. Phys. **66**, 229 (1994).
[39] I. Arad, B. Dhruva, S. Kurien, V. S. L'vov, I. Procaccia, and K. R. Sreenivasan, Phys. Rev. Lett. **81**, 5330 (1998).
[40] I. Arad, V. S. L'vov, and I. Procaccia, Phys. Rev. E **59**, 6753 (1999).
[41] L. Biferale and I. Procaccia, Phys. Rep. **414**, 43 (2005).
[42] A. N. Kolmogorov, J. Fluid Mech. **13**, 82 (1962).
[43] A. M. Obukhov, J. Fluid Mech. **13**, 77 (1962).
[44] G. Stolovitzky, C. Meneveau, and K. R. Sreenivasan, Phys. Rev. Lett. **80**, 3883 (1998).
[45] The condition for the qth-order moments $\langle x^q \rangle$ to be reliably estimated using the measured PDF $P(x)$ is that the peak is clearly seen in the plot of $x^q P(x)$ against x. In the present paper we obtain the upper limit of q as 8.
[46] Y. Li and C. Meneveau, Phys. Rev. Lett. **95**, 164502 (2005).
[47] Y. Li and C. Meneveau, J. Fluid Mech. **558**, 133 (2006).
[48] A. M. Polyakov, Phys. Rev. E **52**, 6183 (1995).
[49] T. Nakano, T. Gotoh, and D. Fukayama, Phys. Rev. E **67**, 026316 (2003).
[50] R. H. Kraichnan, Phys. Fluids **8**, 575 (1965).
[51] G. K. Batchelor, *The Theory of Homogeneous Turbulence* (Cambridge University Press, Cambridge, 1953).